Validation of Ozone Monitoring Instrument nitrogen dioxide columns

E.A. Celarier, E.J. Brinksma, J.F. Gleason, J.P. Veefkind, A. Cede, J.R. Herman, Dimitri Ionov, Florence Goutail, Jean-Pierre Pommereau, J.-C. Lambert, et al.

Validation of Ozone Monitoring Instrument nitrogen dioxide columns

E. A. Celarier,[1] E. J. Brinksma,[2] J. F. Gleason,[3] J. P. Veefkind,[2] A. Cede,[4] J. R. Herman,[3] D. Ionov,[5,6] F. Goutail,[6] J.-P. Pommereau,[6] J.-C. Lambert,[7] M. van Roozendael,[7] G. Pinardi,[7] F. Wittrock,[8] A. Schönhardt,[8] A. Richter,[8] O. W. Ibrahim,[9] T. Wagner,[10] B. Bojkov,[4] G. Mount,[11] E. Spinei,[11] C. M. Chen,[12] T. J. Pongetti,[12] S. P. Sander,[12] E. J. Bucsela,[4] M. O. Wenig,[4] D. P. J. Swart,[13] H. Volten,[2,13] M. Kroon,[2] and P. F. Levelt[2]

Received 2 May 2007; revised 6 November 2007; accepted 30 January 2008; published 7 May 2008.

[1] We review the standard nitrogen dioxide (NO_2) data product (Version 1.0.), which is based on measurements made in the spectral region 415–465 nm by the Ozone Monitoring Instrument (OMI) on the NASA Earth Observing System-Aura satellite. A number of ground- and aircraft-based measurements have been used to validate the data product's three principal quantities: stratospheric, tropospheric, and total NO_2 column densities under nearly or completely cloud-free conditions. The validation of OMI NO_2 is complicated by a number of factors, the greatest of which is that the OMI observations effectively average the NO_2 over its field of view (minimum 340 km^2), while a ground-based instrument samples at a single point. The tropospheric NO_2 field is often very inhomogeneous, varying significantly over tens to hundreds of meters, and ranges from $<10^{15}$ cm^{-2} over remote, rural areas to $>10^{16}$ cm^{-2} over urban and industrial areas. Because of OMI's areal averaging, when validation measurements are made near NO_2 sources the OMI measurements are expected to underestimate the ground-based, and this is indeed seen. Further, we use several different instruments, both new and mature, which might give inconsistent NO_2 amounts; the correlations between nearby instruments is 0.8–0.9. Finally, many of the validation data sets are quite small and span a very short length of time; this limits the statistical conclusions that can be drawn from them. Despite these factors, good agreement is generally seen between the OMI and ground-based measurements, with OMI stratospheric NO_2 underestimated by about 14% and total and tropospheric columns underestimated by 15–30%. Typical correlations between OMI NO_2 and ground-based measurements are generally >0.6.

Citation: Celarier, E. A., et al. (2008), Validation of Ozone Monitoring Instrument nitrogen dioxide columns, *J. Geophys. Res.*, *113*, D15S15, doi:10.1029/2007JD008908.

1. Introduction

[2] The Ozone Monitoring Instrument (OMI) is a space-borne spectroradiometer that uses a two-dimensional charge-coupled device (CCD) array detector to simultaneously measure the spectra of the Earth shine radiance at large number of viewing angles, approximately transverse to the Aura spacecraft's flight track. OMI measures in three broad spectral regions (UV-1, UV-2, and VIS), with a spectral resolution on the order of 0.5 nm. Applying spectral fitting techniques to the OMI data permits the simultaneous retrieval of a wide range of atmospheric trace gas concentrations as well as cloud and aerosol properties and loadings. Among the trace gases that can be retrieved, ozone (O_3) and nitrogen dioxide (NO_2) are identified as essential measurements, both for the ongoing monitoring of the Earth's stratospheric ozone layer and for the monitoring of tropospheric air quality. A more extensive discussion of the OMI instrument itself can be found in the work of *Levelt et al.* [2006b].

[3] The OMI NO_2 data production algorithm is designed to retrieve total vertical column densities of NO_2 and

[1]SGT, Inc., Greenbelt, Maryland, USA.
[2]Royal Netherlands Meteorological Institute, De Bilt, Netherlands.
[3]NASA Goddard Space Flight Center, Greenbelt, Maryland, USA.
[4]GEST Program, University of Maryland, Baltimore County, Baltimore, Maryland, USA.
[5]Department of Atmospheric Physics, Research Institute of Physics, St. Petersburg State University, St. Petersburg, Russia.
[6]CNRS, Verrières le Buisson, France.
[7]Chemistry and Physics of Atmospheres, Federal Space Pole, Belgian Institute for Space Aeronomy, Brussels, Belgium.
[8]Institute for Environmental Physics, University of Bremen, Bremen, Germany.
[9]Institute for Environmental Physics, University of Heidelberg, Heidelberg, Germany.
[10]Max-Planck-Institute for Chemistry, Mainz, Germany.
[11]Laboratory for Atmospheric Research, Department of Civil and Environmental Engineering, Washington State University, Pullman, Washington, USA.
[12]Science Division, NASA Jet Propulsion Laboratory, California Institute of Technology, Pasadena, California, USA.
[13]Netherlands National Institute for Public Health and the Environment (RIVM), Bilthoven, Netherlands.

0148-0227/08/2007JD008908

separate stratospheric and tropospheric column densities; this enables improvement in the calculation of the total vertical column. This separation is important (and possible) because the chemistry and dynamics of NO_2 are different between the stratosphere and the troposphere. Accurate measurements of the tropospheric NO_2 are significant for the characterization of air quality, a primary objective of the Aura and OMI missions.

[4] This paper discusses only the validation of the OMI NO_2 standard product, archived at the Goddard Earth Sciences Data and Information Services Center (GES-DISC). We do not discuss any other product, such as the Level-4 product, archived at the Royal Netherlands Meteorological Institute (KNMI). Furthermore, comparison of OMI to other space borne NO_2 sensors, which all have different equator crossing times from OMI, is beyond the scope of this paper.

[5] A number of efforts toward NO_2 validation have been initiated, in which measurements are made coincident with OMI overpass measurements. The purpose of this paper is to provide an overview of results from these efforts. A variety of instruments and techniques have been used, each with its characteristic sensitivity to stratospheric, tropospheric, or total column NO_2. This paper will address the advantages and, in some cases, the limitations of the various measurements.

[6] Several of the techniques described are new and have not been well-validated. In addition, there is an essential difference between observations of NO_2 taken from the ground and observations averaged over a satellite field of view (FOV). Spatial inhomogeneity, characteristic of airborne constituents emitted at (possibly moving) point sources, and subject to surface-level winds, implies that a single point measurement will often not be a representative sample within a ''collocated'' satellite FOV covering a region of the order of several hundred square kilometers. Monthly average comparisons of ground-based and satellite measurements can remove much of the variability due to FOV-point measurement differences. A preliminary measurement of horizontal inhomogeneity in the NO_2 field is presented in the DANDELIONS overview paper [*Brinksma et al.*, 2008], using a set of simultaneous tropospheric NO_2 measurements made at different azimuths. J. P. Veefkind (private communication, 2007) has shown a comparison of regridded OMI NO_2 data with ground-based observations by the Dutch national air quality network. This network distinguishes regional stations, and city and street stations, which are close to source regions. For the period of the satellite data, NO_2 reported by 35 stations around the Netherlands, averaged between 1100 and 1400 local time, was compared to the collocated OMI measurements. A strong correlation ($R = 0.94$) between the satellite data and the regional station data was found. By contrast, correlations with urban stations are weak because local conditions may vary strongly over a few hundred meters, far smaller than the spatial resolution of OMI. Because of both the novelty of some of the techniques, and such spatial-scale effects, specific results are sometimes limited to qualitative, or order-of-magnitude, conclusions.

[7] Among the validation studies discussed here are ground-based observations made within the SAOZ and DOAS networks (Système d'Analyse par Observations Zénithales and Differential Optical Absorption Spectroscopy instruments, respectively). These are zenith-sky, twilight measurements, which are sensitive to the stratospheric NO_2 column (as explained in section 4.1.1). In addition, the locations are very often pristine areas or at elevation. Even if the instrumentation were sensitive to tropospheric NO_2, the lack of pollution would lead to measurements dominated by the stratospheric NO_2 amount.

[8] To focus on polluted areas, where satellite NO_2 retrievals are most challenging, novel (or as yet unvalidated) techniques must be used.

[9] Measurements of scattered light by the Multiaxial DOAS (MAX-DOAS) technique [*Platt*, 1994; *Wittrock et al.*, 2004], using a range of viewing angles from nearly horizontal through zenith, are sensitive to the tropospheric part of the column, and provide both total and tropospheric NO_2 amounts. We present results from MAX-DOAS measurements taken in a polluted area, but away from immediate local sources, in section 4.2.1.

[10] Direct-sun ground-based measurements, made with a Brewer spectrophotometer [*Cede et al.*, 2006] and with newly developed direct-sun instruments, including a high-resolution ultraviolet Fourier transform spectroscopy (UV-FTS) technique [*Cageao et al.*, 2001], and a number of direct-sun DOAS-type measurements, are sensitive to the total NO_2 column. We will briefly review some preliminary results from these methods in section 4.3.

[11] Validation of the OMI NO_2 data should take account of the sensitivity of the numerous geophysical and geometric algorithmic inputs. These include the a priori profile shapes, surface albedo, and measured and assumed cloud properties. These, in particular, greatly affect the air mass factors (AMF; the ratio of slant-column density of the absorber along the optical path to the vertical column density) the algorithm calculates. Tropospheric NO_2 profiles have been measured with lidar in the Netherlands, during a number of days in September 2006, and with airborne instrumentation during various validation campaigns.

[12] During the Polar Aura Validation Experiment (PAVE) (flights from New Hampshire, January and February 2005) the thermal-dissociation laser induced fluorescence (TD-LIF) instrument [*Thornton et al.*, 2000; *Cleary et al.*, 2002] was used for in situ sampling of NO_2 during the aircraft flights. The NASA DC-8 performed two flight legs at 300 m altitude, near the top of the boundary layer. When flights entered the boundary layer, strongly enhanced concentrations of NO_2 were found.

[13] During the Intercontinental Chemical Transport Experiment, Part B (INTEX-B) campaign (flights from Houston, Texas, March 2006 and from Honolulu, Hawaii, and Anchorage, Alaska, April and May 2006) the TD-LIF instrument measured NO_2 in situ. Spirals were flown by the NASA DC-8 during several flights in spatial and temporal collocation with OMI observations.

[14] Besides INTEX-B, a small number of other airborne campaigns have been carried out, measuring NO_2 in situ, and have been applied to satellite validation [*Heland et al.*, 2002; *Martin et al.*, 2006].

[15] The remainder of section 1 contains a brief description of NO_2 chemistry in the stratosphere and troposphere, the OMI measurement of NO_2, and the availability of the data sets. Section 2 describes the OMI measurement, and section 3 describes the algorithm that reduces the raw OMI

measurements to the various NO_2 columns. The subsections of section 4 discuss the validations of the three principal NO_2 products: stratospheric column (section 4.1), tropospheric column (section 4.2), and total column (section 4.3). The conclusions are presented in section 5.

1.1. Nitrogen Dioxide in the Stratosphere

[16] Nitrogen dioxide participates both directly and indirectly in the catalytic destruction of ozone in the stratosphere [*Finlayson-Pitts and Pitts*, 2000]. Direct catalytic destruction takes place via a NO-NO_2 cycle that catalyzes the reaction $O_3 + O \rightarrow 2O_2$, while while NO_2 concentrations indirectly control ozone loss through other catalytic cycles by controlling, for example, the distribution of chlorine between its catalytically active (ClO) and inactive, reservoir ($ClONO_2$) species.

[17] In the stratosphere, NO_2 concentration has a distinctive diurnal cycle, due largely to the photochemistry of nitrogen oxides. At night, all the photolysis reactions stop, shifting the steady state to NO_2. NO_2 is converted, through ozonolysis, to NO_3, which can further combine with NO_2 to form N_2O_5. This results in a slow decrease of NO_2 over the course of the night. When the air is again sunlit, the N_2O_5 rapidly redissociates to NO_2 and NO_3, which photolyzes instantaneously, mostly to NO. Meanwhile, NO_2 photolyzes very rapidly, and so decreases very rapidly at sunrise. While in daylight, the dominant processes are the interconversion between NO and NO_2. Under most typical conditions of temperature and ozone concentration, latitude, and season, there is a slow increase in NO_2 concentration over the course of the daylight hours. In addition to the chemical and photochemical processes, transport by the winds, particularly in the vicinity of the polar jets may mean that the air that one is measuring has not had the photochemical history one would expect, based on location and local time, alone. Some caution is therefore needed in matching satellite measurements to the ground-based measurements.

1.2. Nitrogen Dioxide in the Troposphere

[18] In the troposphere, nitrogen oxides are a significant contributor to poor air quality. Gaseous NO_2 is red in color and gives rise to the characteristic brownish cast of polluted air. Both NO and NO_2 are harmful to lung tissue, and, as a powerful oxidizing agent, NO_2 is harmful to biological tissue generally. Besides its direct effects, photolysis of NO_2 contributes to ozone production [*Finlayson-Pitts and Pitts*, 2000] according to

$$NO_2 + h\nu \longrightarrow NO + O$$

$$O + O_2 \longrightarrow O_3$$

Nitrogen oxides are produced in high-temperature processes, most notably in combustion (fossil fuels and biomass burning) and in lightning. As a rule, the higher the combustion temperature, the more NOx is produced. Nearly all the NOx ($NO + NO_2$) that is significant for human health is produced by industrial and urban activity, including transportation and power generation.

[19] NO_2 is removed from the troposphere through conversion to HNO_3, nitric acid, which readily dissolves in any available water droplets. NO_2 plumes are detected only up to about 200 km from their source. In the neighborhood of industrial or urban sources, there is a distinct diurnal pattern in the concentration of NOx. The diurnal signal at any location is the result of a complex interplay between the emission source field in space and time, photochemical lifetimes, advection, and the concentrations of chemical sinks for NOx species. As mentioned before, these also give rise to spatial inhomogeneities on a sub-100 m scale. At middle to low latitudes, where a polar-orbiting satellite passes over a given location is only once or twice a day, the satellite only sees a "snapshot" of the state of the polluted atmosphere at the overpass times. In the middle to upper latitudes inconsistent measurements from one orbit to the next, over some location, may well result from significant changes in the NO_2 concentrations over the intervening 100 minutes, as well as from other rapid geophysical changes, e.g., in cloud cover.

1.3. OMI Measurement of NO_2

[20] The Aura satellite is a polar-orbiting, Sun-synchronous satellite, whose orbital period is 99 min. Aura flies over the entire surface of the Earth every 14–15 orbits. Using the two-dimensional CCD array detector, with pixel binning factors chosen to optimize the signal-to-noise ratio, the instrument measures earthshine radiance spectra simultaneously in 60 effective FOVs, approximately transverse to the flight track, every 2 s (the CCD is read out every 0.4 s and coadded in groups of 5), over a range of angles 57° either side of nadir. This gives a sufficient "push-broom" width to view the entire sunlit surface of the Earth, even in the tropics, with multiple orbital overlaps for much of the midlatitude to high-latitude regions.

[21] During normal operations, OMI measures the solar irradiance spectrum once every 24 h. The ratio of the earthshine radiance to solar irradiance, the "spectral albedo," is calculated for each FOV. The OMI NO_2 retrieval algorithm is described in section 3.

1.4. Data Availability

[22] The OMI NO_2 data product is available in a number of different geospatial forms: (1) level-2 orbital swath (L2); (2) daily global gridded, 0.25° × 0.25° (L2G); (3) station and regional overpass (OVP). The L2 and L2G data sets and associated documentation are freely available through the NASA's GES-DISC at http://daac.gsfc.nasa.gov/Aura/OMI/index.shtml.

[23] The OVP data, generated daily for over 100 locations around the world, and also in support of validation and regional pollution studies, are available through the Aura Validation Data Center (AVDC, http://avdc.gsfc.nasa.gov/Data/Aura/OMI/OMNO2/index.html). The subsetted data used for this paper were generated at the AVDC using the recommended usage quality flags [*Celarier et al.*, 2006].

[24] Both the L2G and OVP data products are derived from the L2 data set, and not all of the fields found in the L2 data may be found in the derived data products. Complete details concerning the contents of the Level-2 files are available in the work of *Veefkind and Celarier* [2006].

[25] Each L2G file contains a 0.25° × 0.25° grid data structure. Each cell of the grid contains a stack of data values for all the FOVs whose centers fell within that cell. For each FOV a subset of the available L2 fields is stored.

Because it is organized geographically, the L2G data set should be suitable for users who wish to study specific geographic locations, as, for example, in the case of validation against ground-based measurements or for regional air quality studies. Though all the data have been publicly released and are freely available, prospective data users are strongly encouraged to contact the principal investigators responsible for the data sets.

2. OMI Measurement

[26] Atmospheric NO_2 column densities are retrieved using spectral measurements of the solar irradiance and earthshine radiance in the wavelength region 415–465 nm, using the instrument's VIS detector. The measurements are made with a spectral resolution of ~0.5 nm. Daily measurements of the solar irradiance have been made since the instrument became operational, with the exception of the period 2006 February 28 through 2006 March 3, when a problem with the instrument's folding mirror prevented making daily irradiance measurements. Using measured irradiance spectra has resulted in the appearance of stripe structure in virtually all the data products, in which the retrieved quantities have different means at each of the 60 cross-track positions. This has necessitated the implementation of ''destriping'' algorithms.

[27] The OMI instrument design and performance have been described by *Levelt et al.* [2006a, 2006b]. *Dobber et al.* [2006] have discussed the calibration of the instrument, and the origin of the striping, or cross-track bias.

3. OMI Algorithm

[28] In this section we present the essential details of the algorithm. A much more detailed description of the OMI NO_2 algorithm, its theoretical underpinnings, and uncertainty analysis may be found in the work of *Bucsela et al.* [2006], *Boersma et al.* [2002], *Wenig et al.* [2008] and *Boersma et al.* [2004].

3.1. Slant Column Densities

[29] The first part of the calculation of NO_2 columns consists in calculating the slant column densities (SCD). Since the OMI-measured radiance and irradiance spectra and the laboratory spectra are all measured on different wavelength scales, the measured spectra are interpolated onto a common scale. The spectral albedo, R, is then fitted by a nonlinear least-squares technique onto the function

$$R(\lambda) = P_3(\lambda) \cdot \exp(-c_{\mathrm{NO2}} \cdot \sigma_{\mathrm{NO2}}(\lambda) - c_{\mathrm{O3}} \cdot \sigma_{\mathrm{O3}}(\lambda)) \cdot \left(1 + c_{\mathrm{ring}} \cdot \sigma_{\mathrm{ring}}(\lambda)\right), \quad (1)$$

where σ is the absorption cross section of the indicated species, and P_3 is a third-order polynomial in the wavelength, which models the component of the spectrum that is smoothly varying due to Rayleigh and Mie scattering. Literature spectra are used for σ_{NO2} [*Vandaele et al.*, 1998], σ_{O3} [*Burrows et al.*, 1999a], and σ_{ring} [*Chance and Spurr*, 1997]. These spectra were convolved with a model OMI instrument slit function prior to use in the fitting algorithm. In all, each measured spectrum is subjected to a nonlinear least-squares fit with a total of seven free parameters (c_{NO2}, c_{O3}, c_{ring}, and the four coefficients in $P_3(\lambda)$). The algorithm also estimates the uncertainties in each of the fit parameters, as well as the χ^2 error and root mean square error of the fit.

[30] The determination of the SCD does not include fitting to the absorption spectra of either H_2O or O_2-O_2. The introduction of these species were found not to have a large effect on the retrieved NO_2 SCD and resulted in longer execution times.

3.2. Initial Vertical Column Densities

[31] Initial estimates of the vertical column density (V_{init}) are calculated using AMFs derived from typical climatological profile shapes, with a nominal amount of NO_2 assumed in the troposphere ($\mathrm{AMF}_{\mathrm{init}}$). That is, the initial vertical columns are computed under the assumption that the troposphere is not polluted. The profiles assumed are a 1-year average of daily profiles computed using the GEOS-CHEM model in the troposphere and the Goddard Chemical Transport Model in the stratosphere [*Bucsela et al.*, 2006].

3.3. Stratosphere-Troposphere Separation

[32] At the core of the OMI NO_2 algorithm is a procedure to identify fields of view (FOV) where there is significant tropospheric NO_2. This is required because the air mass factor depends upon the profile shape (though not the total amount, since the trace gas is optically thin): FOVs where there is significant tropospheric NO_2 require a different AMF to compute the vertical column density (VCD) from the SCD. It is observed [*Gordley et al.*, 1996] that the stratospheric NO_2 field has relatively small gradients, particularly in the zonal direction. Our procedure for the stratosphere-troposphere separation essentially identifies the slowly varying component of the total NO_2 field as the stratospheric field and the rest as the tropospheric field.

[33] Each orbit is treated as follows. The ''target'' orbit's data are read in, along with the data from all other available orbits that were measured within ±12 hours of the target. Each FOV is identified with a grid cell on a $1^\circ \times 1^\circ$ grid in latitude and longitude. For all the FOVs that are identified with a particular grid cell, a ''cost'' is computed from the initial AMF and uncertainty estimate for the V_{init}; the value of V_{init} having the lowest cost is saved in its associated grid cell. A ''mask'' identifying grid cells where there are known, persistent sources of NO_2 was developed for use in the algorithm; no V_{init} values are stored in masked grid cells. The V_{init} values are averaged in the meridional direction with a boxcar function of half width 5°. For each 1° latitude band, a wave analysis is performed, fitting waves 0, 1, and 2, to give a preliminary background field. Grid cells whose V_{init} value exceeds the preliminary background field by more than one standard deviation are then excluded and the wave analysis is redone. The result of this is a background field (V_{bg}) that has been influenced very little by the presence of regions of high NO_2 concentration. Since the V_{init} values were obtained using an AMF that is appropriate to a profile having most of the NO_2 in the stratosphere, no further correction to the background field is required.

3.4. Vertical Column Densities

[34] For each FOV, the value of V_{init} is compared to the evaluated background field at that location. If V_{init} is less

than the background field, then the final value of V (the total NO_2 column amount) is taken to be V_{init}. If V_{init} is larger than the background field, then the "polluted" part ($V_{\text{init}} - V_{\text{bg}}$) is scaled by the ratio $\text{AMF}_{\text{init}}/\text{AMF}_{\text{pol}}$, where AMF_{pol} is obtained using the climatological GEOS-CHEM-modeled profile [*Bey et al.*, 2001; *Martin et al.*, 2002]. This procedure gives the total column, the background column, and the polluted column. In addition, a tropospheric column is computed: In the polluted case it is equal to the polluted column plus the amount of the unpolluted profile that exists below the tropopause. In the algorithm, the tropopause is assumed to be at 200 hPa, but moving it to 150 hPa only changes the tropospheric amount by $\sim 1. \times 10^{14}$ cm^{-2}. Finally, if, according to the standard cloud product, the cloud fraction is larger than 0.1, then the "below cloud amount" (the amount of NO_2 that is inferred to be below the visible surface of the clouds) is also computed. This is done by scaling the climatological polluted profile according to the amount of NO_2 that is visible and the reported cloud fraction and cloud top height. (Note, however, that all of the validation studies discussed in this paper used measurements made in cloud-free conditions or nearly so.)

3.5. Destriping

[35] Owing to radiometric calibration and dark-current drift in OMI's CCD detectors (which affects the radiance measurements differently from the irradiance measurements) nearly all OMI Level-2 data products show some degree of cross-track bias, which appears as stripes of systematically elevated or diminished values at certain cross-track scan positions and persisting throughout each orbital track [*Dobber et al.*, 2006]. While the origin of much of the cross-track bias is now understood, and an improvement in the Level-0 to Level-1 processing algorithm is being implemented, the data available for the purpose of validation to date have had significant cross-track bias.

[36] A "destriping" procedure has been implemented in the OMI NO_2 algorithm. In this procedure, the NO_2 SCDs and AMFs are collected for the 15 orbits (or fewer, depending on data availability) used to construct the background field. These are then used to construct separate SCD correction offsets for the northern and southern hemispheres:

$$\Delta_i = \overline{\text{SCD}_i} - \overline{\text{AMF}_i} \cdot \frac{\langle \text{SCD} \rangle}{\langle \text{AMF} \rangle}, \tag{2}$$

where i is the cross-track scan position (1 to 60), the overlines indicate averages for single scan positions, and angle brackets indicate averages over all scan positions. The Δ_i are subtracted from the SCDs before applying the final air mass factors.

[37] One concern about this procedure has been that it could introduce an unknowable bias in the computed NO_2 column densities. This will be discussed in light of the ground-based validation data. Another concern is it is observed that even using this procedure, there is some residual striping in the data. The data that have severe bias are generally flagged (and so not used in the validation). We assume that the residual biases are small, and are sufficiently symmetrically distributed, that the biases cancel: The cross-track biases change from orbit to orbit, and successive overpasses of any site are viewed with different FOVs.

4. Validation of OMI NO_2 Columns

4.1. Stratospheric Column

4.1.1. SAOZ and DOAS Instruments in the NDACC Network

[38] The Network for the Detection of Atmospheric Composition Change (NDACC) is an international cooperative network that coordinates the operations and data analysis at more than 30 stations at various latitudes on the globe from 76°S to 79°N. The ground-based UV-visible zenith-sky spectrometers include SAOZ as well as DOAS instruments, which provide ozone and NO_2 vertical columns at sunrise and sunset using the DOAS technique [*Platt*, 1994] in the spectral range 410–530 nm. Zenith-sky measurements made at solar zenith angles between 86 and 91° are averaged to give estimates of the column NO_2. Because of the optical geometry of the measurement, the retrieved NO_2 column is much more sensitive to the stratospheric NO_2 column than to the tropospheric column. Most of the instruments are located in remote geographical regions, far from any significant source of tropospheric NO_2. Figure 1 shows the geographical distribution of the SAOZ stations that are operated by the French Centre National de la Recherche Scientifique (CNRS). Only the instruments at the Observatoire Haute-Provence (OHP), France, and Bauru, Brazil, are in any proximity to presumed anthropogenic sources of NO_2. Measurements from the SAOZ instruments have been previously used to compare with NO_2 measurements by the space-borne Global Ozone Monitoring Experiment (GOME) [*Burrows et al.*, 1999b] and Scanning Imaging Absorption Spectrometer for Atmospheric Chartography (SCIAMACHY) [*Bovensmann et al.*, 1999] instruments [*Ionov et al.*, 2006a, 2006b, 2007; *Piters et al.*, 2006; *Lambert et al.*, 2001].

[39] Stratospheric NO_2 exhibits a pronounced diurnal cycle due to its daytime photolysis into NO and nighttime conversion into N_2O_5. The NO_2 daily cycle starts with a fast drop shortly after sunrise, followed by a quasi-linear slow increase during the day, a fast increase at sunset, and finally a slow decrease during the night. The time-dependence of the stratospheric NO_2 concentration has important implications for the validation of the space-based NO_2 measurements. If the ground-based measurements are not collocated in time with the OMI measurements, they need to be corrected, using photochemical and transport models, to account for the time difference. In addition, if the ground-based measurements entail an optical path that is more horizontal than vertical, view and solar geometries must be taken into consideration when identifying "collocated" measurements.

[40] The diurnal cycle has been simulated with a photochemical box model derived from the SLIMCAT 3D chemical-transport model [*Denis et al.*, 2005]. It includes 98 chemical and 39 photochemical reactions, including heterogeneous chemistry on liquid and solid particles. Calculations are made at 17 altitude levels with a time step of 1 min. The NO_2 total column is obtained by integrating the profile assuming a constant density in each layer. Figure 2 shows the results of simulations at two SAOZ stations, OHP at

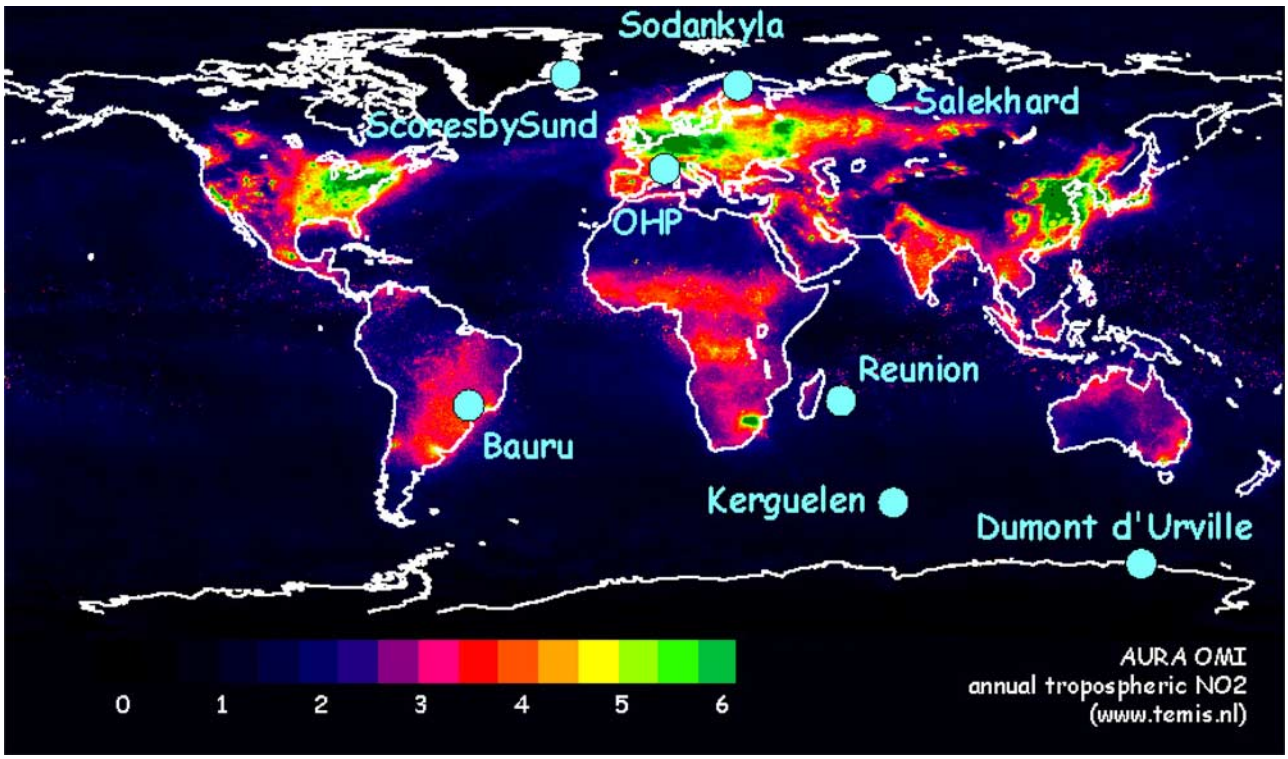

Figure 1. Geographical distribution of eight CNRS-operated SAOZ stations in the NDACC network. The colored field presented is the annual mean tropospheric NO_2 column amounts, as measured by OMI. The color scale units are 10^{15} cm^{-2}.

midlatitude and and Scoresby Sund in the Arctic, for spring and fall. Using this photochemical model, a diurnal time series of the ratio NO_2(sunrise)/NO_2(t) was calculated for each month and at each SAOZ location. As SAOZ is an average of measurements between solar zenith angles (SZA) 86° and 91° the NO_2 column at SZA = 88.5° is taken as the sunrise reference. The OMI stratospheric measurements (total minus tropospheric columns) were calculated and then normalized to corresponding sunrise values using these ratios.

[41] The optical geometry of the twilight SAOZ measurements is such that the light paths traverse rather large distances through the stratosphere, so the stratosphere is sampled at some distance from the measurement site. This should be taken into account when seeking "match up" satellite FOVs corresponding to the ground-based measurements, especially in regions with large stratospheric NO_2 gradients. However in the present studies a simpler approach was adopted, in which the match up criterion was that the ground site was within an OMI FOV. If multiple match ups were identified for a single day, the one whose center fell closest to the ground station was used.

[42] Finally, the OMI NO_2 algorithm provides total column NO_2 and the tropospheric column NO_2. Since SAOZ measurements are roughly 20 times as sensitive to the stratospheric column as to the tropospheric column, it is of interest to compare the SAOZ-derived values to the difference of the total and the tropospheric columns.

[43] Figure 3 shows the time series of the difference between the sunrise SAOZ measurements and the matching OMI measurements from eight SAOZ sites, adjusted to account for the difference between the satellite overpass time and sunrise. The statistical characteristics of these differences are presented in Table 1. Besides a comparison to just the stratospheric column, the table presents a comparison between the OMI total column and the SAOZ instrument measurements. At virtually all latitudes the agreement between the ground-based and satellite-based measurements of the total stratospheric NO_2 column is rather good (average RMS difference $\sim$ 25%), considering the estimated accuracy estimates of both measurements. However, a small annual cycle is apparent in the time series for the higher latitudes, with lower values in the winter than in the summer. This cycle, which appears in both the northern and southern hemisphere high latitudes, may be related to the OMI sampling under those conditions, may reflect a sensitivity to the choice of matching OMI FOV corresponding to a given ground-based observation, or may be due to a bias either in the satellite measurement at high solar zenith angle or in the ground-based measurements as the sunrise azimuth tends poleward. While the influence of the seasonal cycle on the overall statistics is fairly small, understanding it may be an avenue of further study.

[44] The correlation coefficients between the SAOZ and OMI-measured stratospheric NO_2 columns are better, and the mean absolute differences smaller, for the midlatitude to high-latitude sites than for the tropical sites. Since the stratospheric NO_2 concentrations are smaller in the tropics in the first place (annual mean of about 2.5×10^{15} cm^{-2}, compared to an annual mean of $4-5 \times 10^{15}$ cm^{-2} at the high-latitude sites), the relative differences are much greater

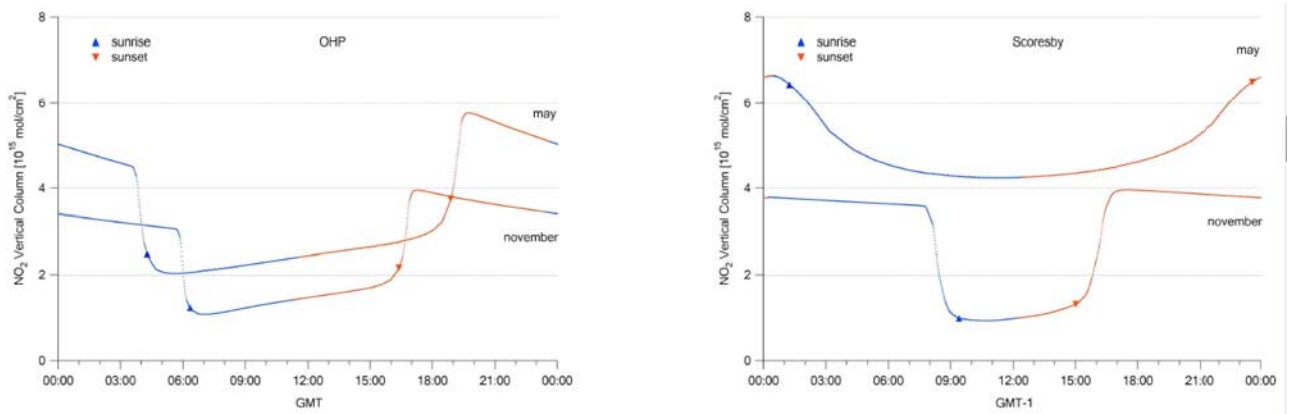

Figure 2. Simulated time-history of stratospheric NO_2 at a midlatitude station (OHP) and a high-latitude station (Scoresbysund) for spring and fall. Blue curves represent times before local apparent solar noon. Triangles indicate times of sunrise and sunset.

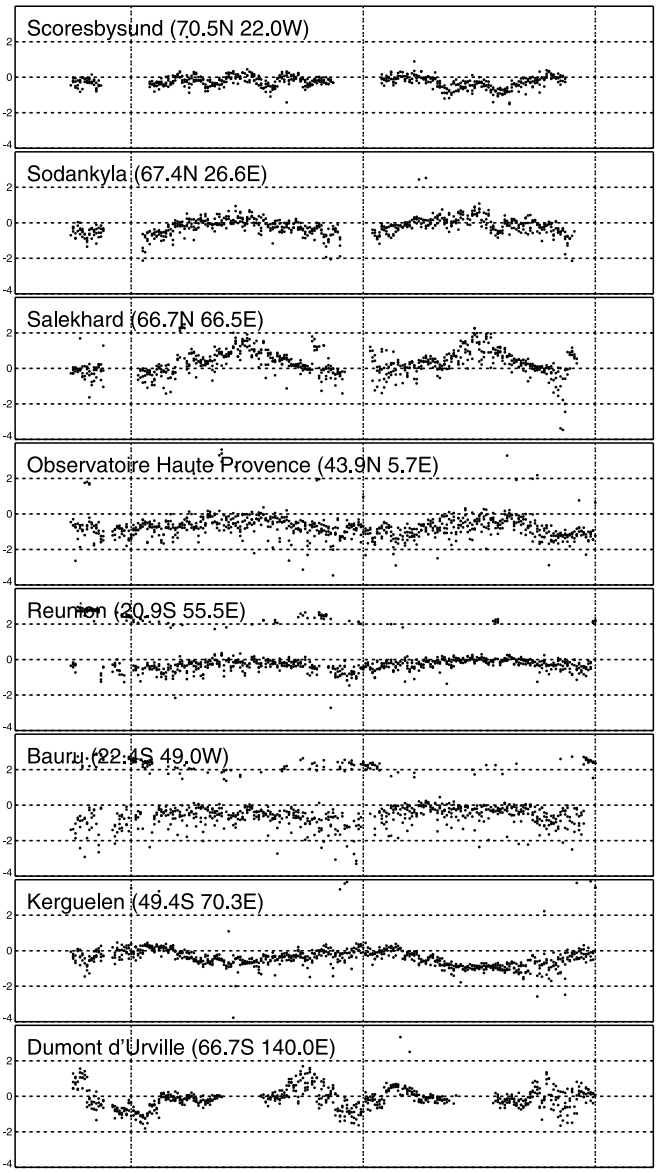

Figure 3. Time series of the difference between OMI and SAOZ-measured stratospheric NO_2 in units of 10^{15} cm^{-2}. The sites are ordered from north to south.

Table 1. Absolute (abs.) and Relative Differences of Average (Δ) and RMS (ρ) and Correlation Coefficients (R) Between Ground-Based SAOZ Measurements and OMI Data Adjusted to Sunrise Using a Photochemical Model (See Text)[a]

	OMI Total – SAOZ					OMI Stratospheric – SAOZ				
	Δ		ρ			Δ		ρ		
Station	abs.	%	abs.	%	R	abs.	%	abs.	%	R
Scoresby Sund	0.02	−0.4	0.82	45.3	0.93	−0.33	−13.9	0.44	20.0	0.99
Sodankyla	0.59	19.2	2.03	93.9	0.71	−0.28	−15.7	0.56	26.6	0.97
Salekhard	1.05	44.1	1.58	72.8	0.86	0.24	4.1	0.73	24.8	0.95
OHP	1.46	52.6	2.41	84.5	0.45	−0.72	−27.5	0.96	33.4	0.68
Reunion	0.18	8.6	0.72	31.5	0.34	−0.44	−15.7	0.54	18.5	0.71
Bauru	0.58	22.8	1.98	69.2	0.18	−0.80	−25.1	0.98	28.6	0.58
Kerguelen	−0.04	−3.8	0.58	20.6	0.88	−0.37	−15.2	0.59	22.7	0.90
Dumont d'Urville	0.26	12.7	1.13	34.5	0.88	−0.23	−2.2	0.67	20.0	0.96
Overall	0.53	19.9	1.56	62.0	0.69	−0.37	−14.3	0.71	25.0	0.91

[a]Absolute and relative differences of average and RMS are measured in units of 10^{15} cm^{-2}. Data from November 2004 through December 2006 were used. We present comparisons with both OMI total and stratospheric NO_2 columns.

in the tropics, and even the midlatitude sites (OHP and Kerguelen), than at the high-latitude sites.

4.2. Tropospheric Column

4.2.1. MAX-DOAS

[45] The Multiaxis DOAS (MAX-DOAS) technique is an extension of the zenith-sky DOAS technique described in section 4.1.1 but having much greater sensitivity to lower tropospheric layers. In brief, a MAX-DOAS typically consists of two main parts: a grating spectrometer mounted inside a thermostatted box that is located inside a building, and one or more scanning telescopes connected to the spectrometer via fiber optics. Consecutive measurements at increasing elevation angles are performed in an acquisition cycle that always contains observations at a number of low elevations and a zenith observation.

[46] From each of the measurements, a slant column is retrieved using the DOAS method described in section 4.1.1 [*Platt*, 1994]. Besides NO_2, a number of other absorbers, plus the Ring effect, are included in the fit, as are a multiplicative polynomial and an additive polynomial for stray light correction. In order to account for the temperature dependence of the NO_2 absorption spectrum, a second cross section (295 K and 221 K) may be introduced in the retrieval to improve the fit and correct the derived vertical column. Some groups use one-temperature retrievals while other groups use two-temperature retrievals, and this may cause some discrepancy between the MAX-DOAS instrument results. In contrast, the OMI retrieval uses a single temperature and applies a height-dependent temperature correction, based on climatological temperature profiles, in the calculation of the AMFs [*Bucsela et al.*, 2006; *Boersma et al.*, 2002].

[47] The lowest-elevation measurements have a large sensitivity to absorption in the boundary layer, while the zenith measurements are used as background reference spectra which contain Fraunhofer structures and the stratospheric absorption features. Since photon scattering largely occurs below the tropopause, the photons collected from different elevation angles have essentially the same stratospheric path, but different light paths in the troposphere. The difference between successive off-axis line-of-sight (LOS) and zenith measurements is therefore only sensitive to the troposphere. For NO_2 retrieval, radiative transfer simulations show that under polluted conditions, the stratospheric contamination is generally smaller than 1%. A more in-depth description of the MAX-DOAS measurements, as they were done at the DANDELIONS campaign, can be found in the work of *Brinksma et al.* [2008].

[48] During the DANDELIONS campaigns [*Brinksma et al.*, 2008], various MAX-DOAS instruments operated quasi continuously from the Cabauw Experimental Site for Atmospheric Research [*Russchenberg et al.*, 2005] throughout May through mid July 2005 and throughout September 2006. These instruments were provided and operated by the Belgian Institute for Space Aeronomy (BIRA-IASB), the University of Bremen, and the University of Heidelberg.

[49] The Heidelberg MAX-DOAS instrument differs from the others in that it has a set of three movable telescopes, which enable simultaneous measurement cycles in three azimuth viewing directions [*Wagner et al.*, 2004].

[50] For the Bremen instrument [*Wittrock et al.*, 2004], the zenith direction is viewed without a mirror, while the other elevation angles in the measurement cycle are selected through a rotating mirror inside the telescope. The range of elevation angles is 0°–30°. In the 2006 DANDELIONS campaign, separate UV and VIS instruments were operated by the Bremen group.

4.2.2. Agreement Between MAX-DOAS Instruments

[51] The level of agreement achieved between the MAX-DOAS instruments is quantitatively summarized in correlation plots (Figure 4) where tropospheric NO_2 columns from the BIRA instrument are compared to those from the other groups for the 2005 campaign. This comparison is useful because there are differences between the instruments and their data reduction procedures and because instruments viewing different directions can be used to detect directional dependences of the measurements. Very good agreement is found between the BIRA and Bremen data sets (correlation coefficients of 0.9 and slope of 1.1), and also between BIRA and the three Heidelberg telescopes (correlations between 0.82 and 0.91), especially considering that the BIRA instrument was 200 m away from the other two instruments.

[52] In Figure 4, the BIRA and Heidelberg data sets were retrieved using identical NO_2 absorption cross sections, rather than each group using its own set of cross sections. This improves the correlation coefficient very slightly (0.91 to 0.92) but improves the slope a great deal (0.78 to 0.93). Notably, there is little improvement in the correlation or the regression slope in the comparisons of the BIRA instrument

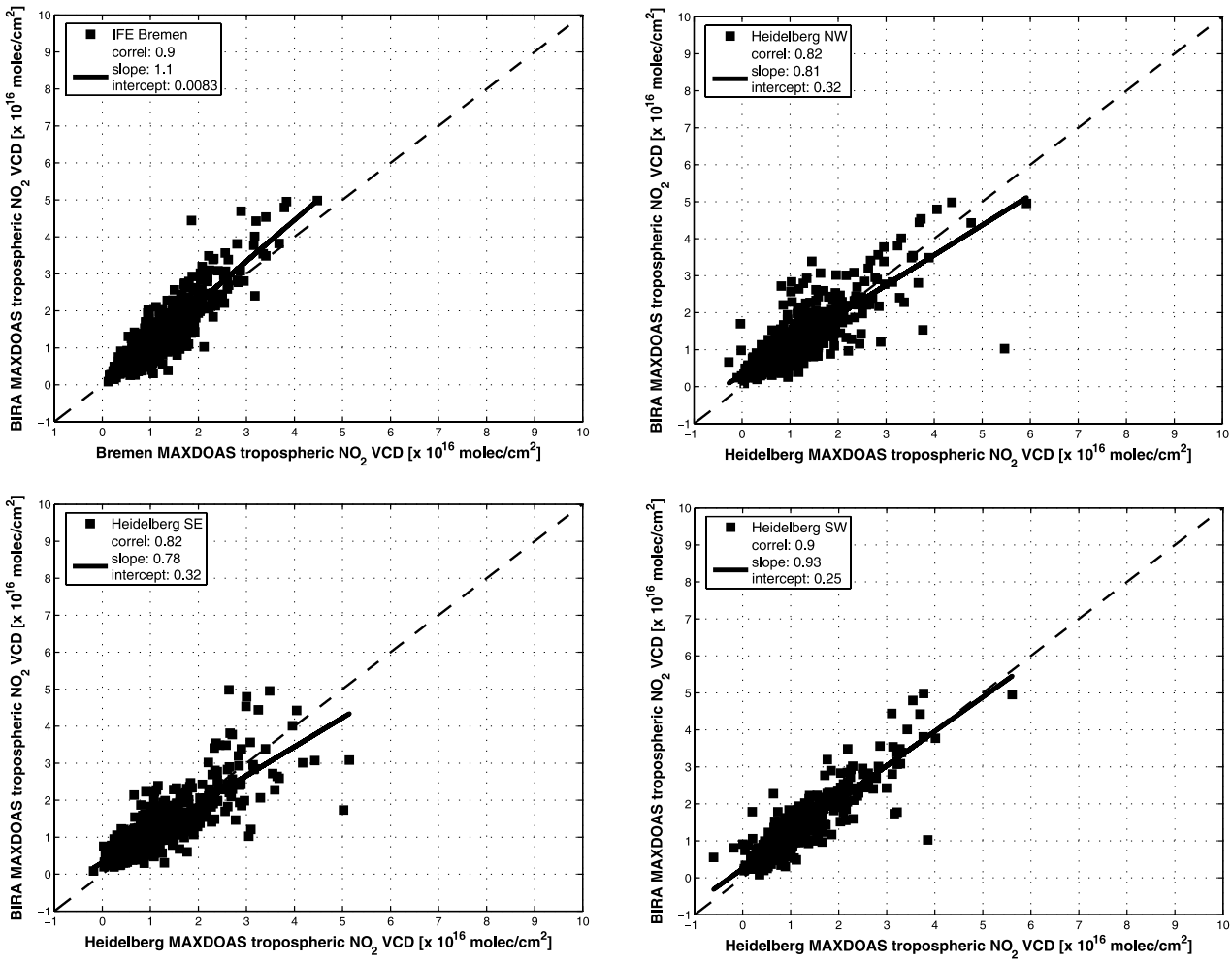

Figure 4. Scatterplots of the tropospheric NO_2 columns retrieved during the 2005 campaign from the BIRA MAX-DOAS instrument and the Bremen MAX-DOAS (top left), the Heidelberg MAX-DOAS for the three pointing directions northwest (top right), southeast (bottom left), and southwest (bottom right), respectively. The regression analysis parameters are given in the legends. For these analyses, the retrievals were all done using identical NO_2 cross sections (see text). The agreement between the BIRA and Heidelberg SW observations are not as good (slope = 0.78, intercept = 0.23) when each group used its own NO_2 cross sections. The correlations between the BIRA and Heidelberg NW and SE instruments are considerably worse than between the BIRA and Heidelberg SW instruments, which point roughly the same direction. This strongly suggests the importance of inhomogeneity of tropospheric NO_2 in the intercomparison of ground-based measurements.

with the other two Heidelberg instruments. This highlights the degree to which horizontal inhomogeneities in the NO_2 field can strongly affect the agreement among ground-based instruments,and strongly suggests that these inhomogeneities are great enough to affect comparisons between the ground-based and satellite-based measurements.

4.2.3. Heterogeneity of the NO_2 Field

[53] If the tropospheric NO_2 layer were horizontally homogenous, the observed NO_2 SCDs for the different azimuth angles observed from the three telescopes of the Heidelberg instrument would have been similar. The horizontal inhomogeneity of the NO_2 concentration field can be estimated from the observed differences among the various viewing directions. Estimating the horizontal inhomogeneity is very important for the validation of satellite instruments with ground-based observations. In the presence of strong horizontal gradients, ground-based observations may not be representative for the average value within a satellite ground pixel.

[54] Since the horizontal extent of the absorption paths along the line of sight is largest for low telescope elevation, those at 3° were used to estimate the heterogeneity of the tropospheric NO_2 concentration field. This was done by evaluating the SCD in the three azimuthal viewing directions at 3° elevation and calculating the ratio of the maximum and the minimum. A horizontally homogenous concentration field yields a ratio of one; the more this ratio deviates from unity, the larger the horizontal gradients. In addition to the strength of the horizontal gradients, the direction of the NO_2 gradient was estimated, though in a limited way, since the Heidelberg MAX-DOAS was measuring in only three azimuth directions. Figure 5 displays

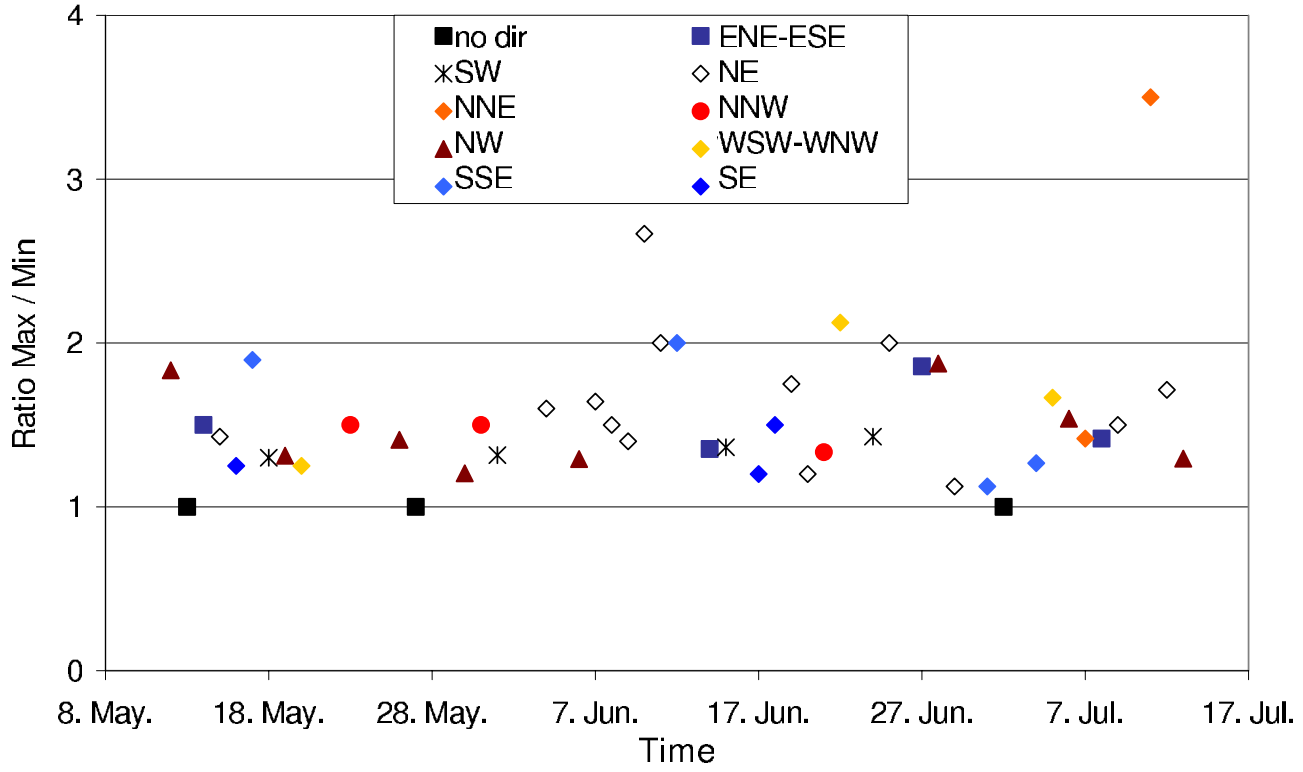

Figure 5. Maximum and minimum NO_2 SCD observed for an elevation angle of 3° of the Heidelberg MAX-DOAS telescopes observing under three different azimuth angles at Cabauw during the dandelions campaign in 2005. High ratios indicate large horizontal gradients of the tropospheric NO_2 concentration field and colors indicate the direction of the gradient (directed toward higher values).

the time series of the ratios at daily noon. High ratios indicate strong gradients, and the color of the points indicates the direction of positive gradient.

[55] To interpret the retrieved information on the gradient of the tropospheric NO_2 concentration field, it is important to consider two effects that can affect the observed SCDs, especially for low elevation angles: First, the sensitivity to the relative azimuth angle (between the telescope and the Sun). This dependency becomes more pronounced for increasing SZA and increasing aerosol load [*Wagner et al.*, 2004]. Second, the effect of the atmospheric aerosol load on the atmospheric visibility and thus on the horizontal extents of the absorption paths along the line of sight. Thus, depending on the aerosol load, the calculated ratio represents information on gradients over areas of different horizontal extent. The dependence on the azimuth angle was found to be below 15% for SZA between 20° and 80°. Almost all observed ratios of the maximum and minimum NO_2 SCDs (see Figure 5) were much larger than this. Effective path lengths are enhanced by aerosols above about 1 km and diminished by aerosols below 1 km. For an elevation angle of 3°, the effective path length is about 19 km in a pure Rayleigh-scattering atmosphere; this can be reduced to as little as 4.5 km by surface-level aerosols, or enhanced to 25 km by higher-altitude aerosols [*Brinksma et al.*, 2008; *Deutschmann and Wagner*, 2006; *Wagner et al.*, 2004, 2007].

4.2.4. Comparisons With OMI Tropospheric NO_2

[56] The different MAX-DOAS data sets are compared to the OMI Level-2 cloud-free data (O_2–O_2 cloud fractions in the OMI products less than 20%) for 2005 in order to produce the correlation plot presented in Figure 6 and Table 2. The MAX-DOAS data were linearly interpolated to the satellite overpass time.

[57] The OMI tropospheric vertical columns were generally distributed from 0 to about 2.5×10^{16} cm^{-2}. In one case the ground-based MAX-DOAS column (3×10^{16} cm^{-2}) significantly exceeded the corresponding satellite value, possibly due to a local enhancement of the NO_2 concentration at Cabauw. Because of its obvious anomaly, this point has been excluded from the regression analysis.

[58] The regression analyses show that similar results were achieved with the BIRA and the Bremen data sets, with the correlation coefficient between ground-based and satellite data being about 0.6. A lower correlation was obtained with the Heidelberg data when considering only the southwest direction measurements (closest to the viewing direction of both Bremen and BIRA instruments), possibly due to the smaller number of coincidences with this instrument and also the shorter integration time used, which may increase the sensitivity to local inhomogeneities in the NO_2 field. In order to further explore the impact of possible horizontal smoothing effects on the comparison results, the Heidelberg measurements simultaneously recorded from all three directions have been averaged and again compared with satellite data. The resulting correlation coefficients, also given in Table 2, have significantly improved and are now the highest of the three MAX-DOAS instruments. This suggests that the scatter in MAX-DOAS

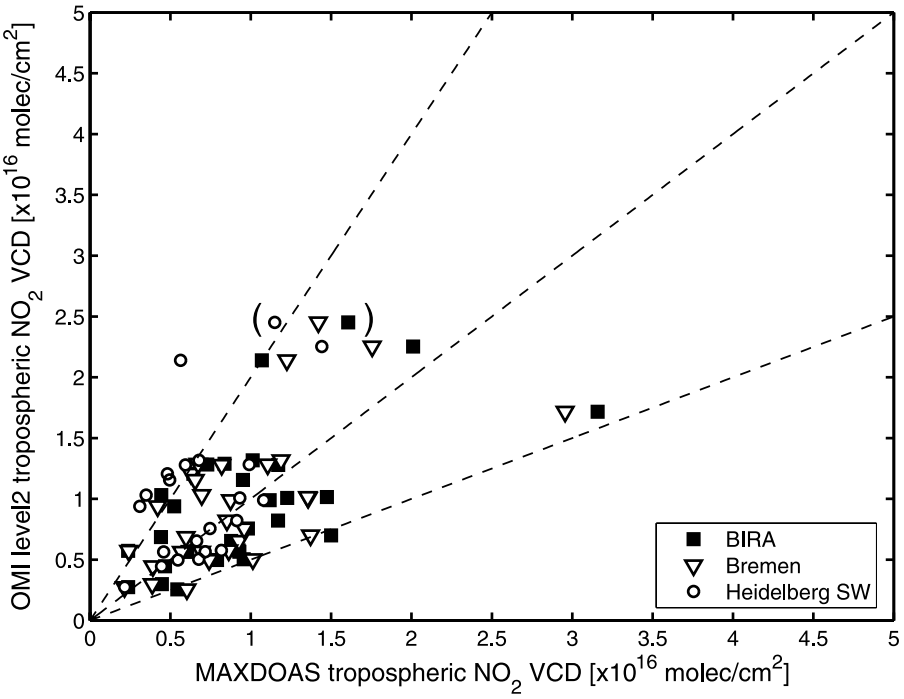

Figure 6. Correlations between tropospheric NO_2 from the three MAX-DOAS instruments at Cabauw (BIRA, Bremen, and Heidelberg SW direction) and OMI Level-2 OMI data are included if cloud fractions were less than 20%. Correlation and regression coefficients are summarized in Table 2. The dashed lines are provided as a visual aid and show slopes of 1/2, 1, and 2. The data point in brackets is clearly an outlier (see text) and was not included in the regression analysis presented in Table 2.

versus satellite comparisons is, indeed, largely dominated by the difference in their spatial and temporal averaging.

[59] As is evident from the regression results the OMI tropospheric NO_2 columns seem to be systematically lower than the MAX-DOAS results for both OMI products considered. It must be noted, however, that the correlation coefficients are rather poor in all cases; possible causes for this include uncertainties in both ground-based data (which use a geometrical approximation for the AMF) and satellite retrievals (e.g., sensitivity of the AMF to aerosols, clouds and NO_2 profile shape). The slopes are poorly determined due to the small number of points and the large data scatter.

4.2.5. Multifunction DOAS Measurements

[60] The Multifunction DOAS (MF-DOAS) instrument observes scattered skylight with a 1° vertical × 0.025° horizontal FOV at varying azimuth and elevation viewing angles and direct sunlight in the UV-visible spectral region. From these measurements are retrieved NO_2, O_3, SO_2, and CH_2O slant columns. The instrument brings together in a single platform direct Sun observations, with their simple air mass factor computation, the zenith scattered sky observations pioneered by Noxon in the 1970s [e.g., *Noxon*, 1975], and the MAX-DOAS observations of low elevation angle scattered sky that emphasize the tropospheric contribution to total column [e.g., *Wittrock et al.*, 2004] with a complex interpretation of air mass factor. The MF-DOAS spectrograph is a substantially modified single pass commercial Czerny-Turner spectrograph of focal length 300 mm. The instrument covers a wavelength range from 280 nm to 490 nm with a spectral resolution of 0.82 nm, and samples at 6 CCD pixels/FWHM. Scattered sky light is collected by a 12 cm telescope and passes into the spectrograph through two filter wheels that contain optional depolarizers, spectral flattening filters UV bandpass, and UV cutoff filters. Direct sunlight is fed into a spectralon 8 cm diameter integrating sphere before passing through the filter wheels and results in a signal level similar to that from the scattered sky. The integrating sphere provides uniform illumination of the spectrograph optics. A two-dimensional CCD detector (512 × 2048 pixels) is used in the focal plane. The typical integration time required to fill the CCD wells is less than 1 s, resulting in excellent signal to noise ratio, even with the integrating sphere that is used to minimize problems with

Table 2. Summary of Statistical Analyses of Comparisons Between Tropospheric NO_2 From MAX-DOAS Data and OMI Level-2[a]

	N	R	Intercept	Slope	RMS Difference	Relative RMS Difference
BIRA south	29	0.60	4.29	0.52	4.82	52%
Bremen southwest	29	0.63	3.93	0.59	4.44	48%
Heidelberg southwest	21	0.45	4.27	0.8	5.38	56%
Heidelberg spatial average	21	0.65	1.99	0.85	3.89	40%

[a]N denotes number of collocations, and R is the correlation coefficient. The intercept and (absolute) RMS difference are in units of 10^{15} cm^{-2}.

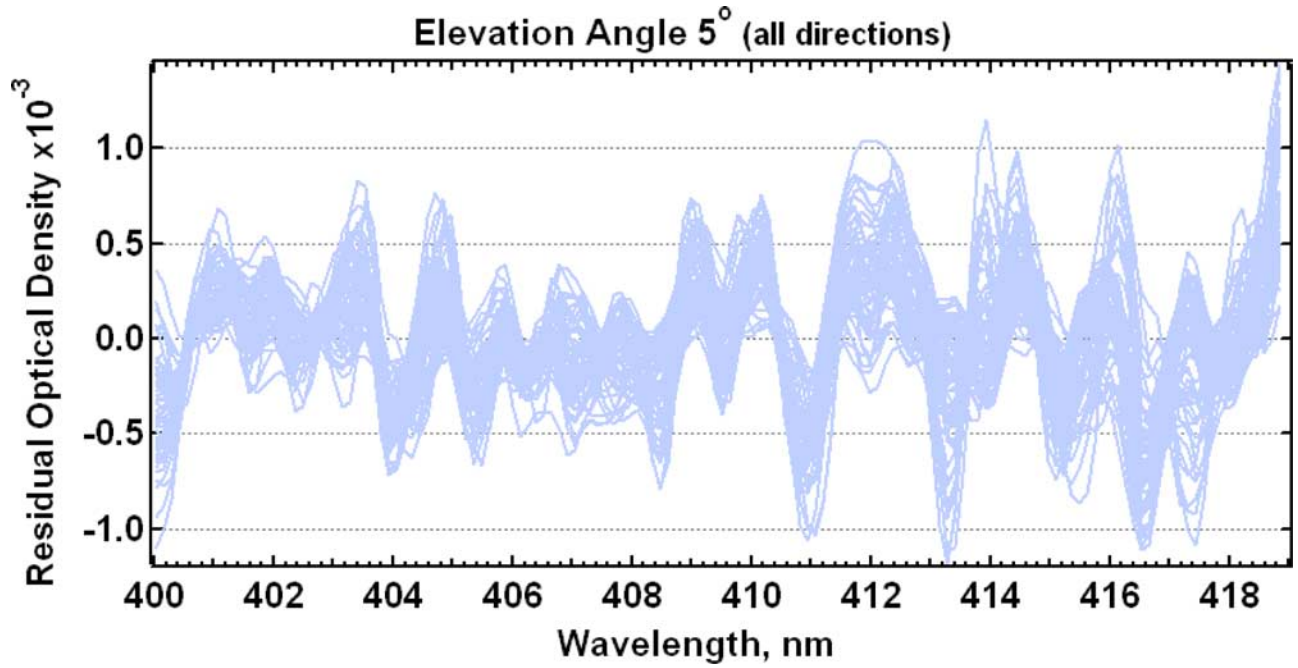

Figure 7. Representative residual optical densities for observations of 9 May 2006 at 5° elevation and four azimuth angles. Residuals are small (~0.1% peak-to-peak) and are caused by both instrumental and geophysical spectral structure.

illumination of the optics. Spectrograph stray light is reduced by a spectral flattening filter, which reduces the long wavelength throughput of the instrument relative to the short wavelength signal. A solar tracker moves the entire instrument for elevation/azimuth positioning and for Sun tracking.

[61] A prototype ground-based MF-DOAS instrument was fielded during the INTEX-B campaign for Aura/OMI validation. It was located at the Pacific Northwest National Laboratory in Richland, Washington (PNNL; 46.3409°N, 119.2787°W), in an urban area known as Tri-Cities (the merged cities of Kennewick, Pasco, and Richland, Washington) with total population of approximately 150,000 in an area of 250 km^2. PNNL is situated approximately 15 km north of the center of Richland and northwest of the area's population center. The major source of local NO_2 pollution is vehicular exhaust, which expected to give rise to pronounced diurnal and weekly cycles.

[62] NO_2 differential slant columns (DSCD) were derived using the DOAS technique based on Beer's law. A nonlinear least squares algorithm was used to fit the measured spectral cross sections of NO_2, O_3, instrument spectral polarization, and Ring effect in the spectral region 400–419 nm. A polynomial was included to model the slowly varying Rayleigh and Mie scattering spectral shapes. The reference solar spectrum used for the data analysis was measured at zenith at local noon on 30 April 2006, a day with very low pollution levels. Raw spectra were corrected for detector dark background and flat field.

[63] Figure 7 shows typical residual optical densities after the least squares fitting procedure for observations taken on 9 May 2006 at 5° elevation and four azimuth angles. The LIDORT radiative transfer code [*Spurr*, 2001; *Spurr et al.*, 2001] was used to calculate the AMF to convert the DSCD to VCD.

[64] As an example of the results, Figure 8 presents the spatial and temporal variation of NO_2 differential slant column for 9 May 2006, a polluted day. Higher column densities were observed to the south and east, toward the urban center, as expected. Measurements taken at 5° elevation showed higher NO_2 tropospheric column compared to 15° and 45° angles, as expected. These elevated NO_2 slant column densities were particularly pronounced during the morning rush hour.

[65] Figure 9 shows contour plots of OMI tropospheric NO_2 VCD for 9 May, derived from the Level-2 OMI data product. OMI tropospheric NO_2 vertical column densities "integrated" over several pixels in the MF-DOAS observation direction were compared to MF-DOAS tropospheric NO_2 VCD using a priori differential AMFs for clear days at PNNL from the LIDORT radiative transfer code.

[66] Figure 10 shows results for the time period 30 April through 13 May 2006, with reasonable correlation observed for these clear days. The slope of the data in Figure 10 shows that OMI determinations of tropospheric NO_2 VCD are 0.81 ± 0.11 of those determined from MF-DOAS with a coefficient of determination R^2 of 0.92.

4.3. Total Column

4.3.1. Brewer

[67] *Cede et al.* [2006] have described a method for retrieval of total-column NO_2 from direct-Sun measurements using a Brewer MK-III double monochromator spectrophotometer. The Brewer MK-III instrument was primarily designed to make measurements of ozone from wavelengths below 320 nm and can measure spectral irradiance and radiance from 285 to 365 nm. Its measure-

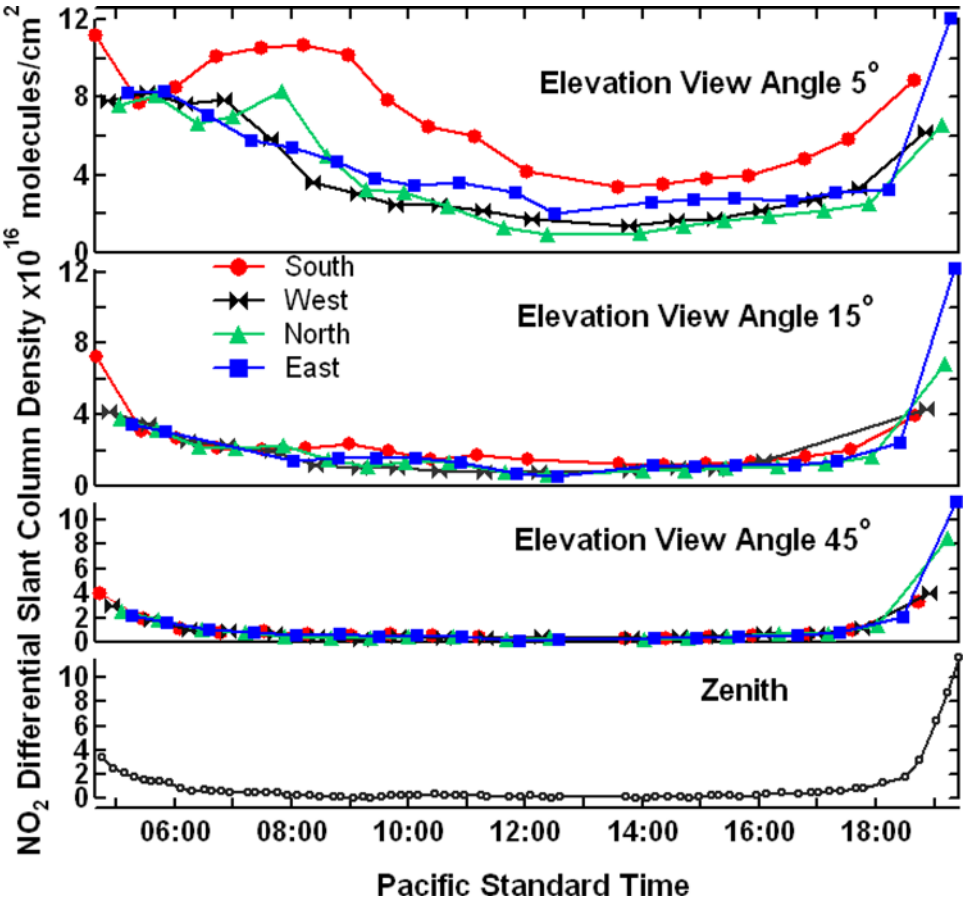

Figure 8. Example of measured spatial and temporal variation of MF-DOAS-measured NO_2 differential SCD for 9 May 2006.

ment modes include a spectral scan mode, where the gratings are moved and any wavelength can be selected, and a slit mask mode, in which a slit mask is introduced in the optical path allowing nearly simultaneous measurements at six wavelengths, spaced about 3 nm apart.

[68] The spacing of the slits in the slit mask was chosen to optimize the ozone retrievals between 303 and 320 nm, but in the 345–365 nm range the measured wavelengths fall very nearly on maxima and minima in the NO_2 absorption spectrum (see Figure 11), which permits the retrieval of total column NO_2. These measurements have been made at the NASA Goddard Space Flight Center on a nearly continual basis since August 2004, with measurements made every half hour during the sunlit hours.

[69] The retrieved NO_2 columns have a large instrumental noise, so data must be averaged over several hours time in order to make meaningful comparisons to the OMI-measured values. However, the location of the instrument (3 km from the Washington Capital Beltway and 2 km from the Baltimore-Washington Parkway, on the outskirts of a major metropolitan area) is such that there are often substantial subhour time variations in the actual tropospheric NO_2 concentrations. The combination of the intrinsic variability of the measurements with the frequent occurrence of significant actual concentration variations within a given time window used for collocation with OMI overpasses complicates the process of using the Brewer data for validation of OMI NO_2 measurements. Comparisons having useful statistical significance can be made using monthly averages of the Brewer and OMI data sets.

[70] Figure 12 shows the comparison between the monthly mean Brewer-measured and OMI-measured NO_2 columns. In the Washington DC area, early afternoon NO_2 columns are dominated by the boundary layer columns. The difference that is seen with OMI-measured columns that are about 35% smaller than the Brewer-measured columns can thus be largely attributed to the tropospheric NO_2.

[71] In Figure 13 the daily and monthly mean values are plotted, along with the line of linear regression to the monthly means. The regression analysis, performed on the monthly means, and weighted according to the standard deviations, gives a slope of 0.70.

4.3.2. Pandora-1 Direct Sun DOAS Measurements

[72] The lightweight, portable Pandora-1 spectrometer system measures direct-Sun irradiances from 270 to 500 nm at ~0.5 nm resolution. The outdoor head sensor is mounted on a tracking system and holds a single strand fiber optic cable, which collects the light passed through a collimator (1.6° FWHM field of view) and a filter wheel. The other end of the fiber is connected to a 75 mm focal length symmetric Czerny-Turner grating spectrometer using a 1024 × 1 pixel complementary metal oxide semiconductor (CMOS) detector, temperature stabilized to 20° ± 1. The total NO_2 column is retrieved by the DOAS method, in the

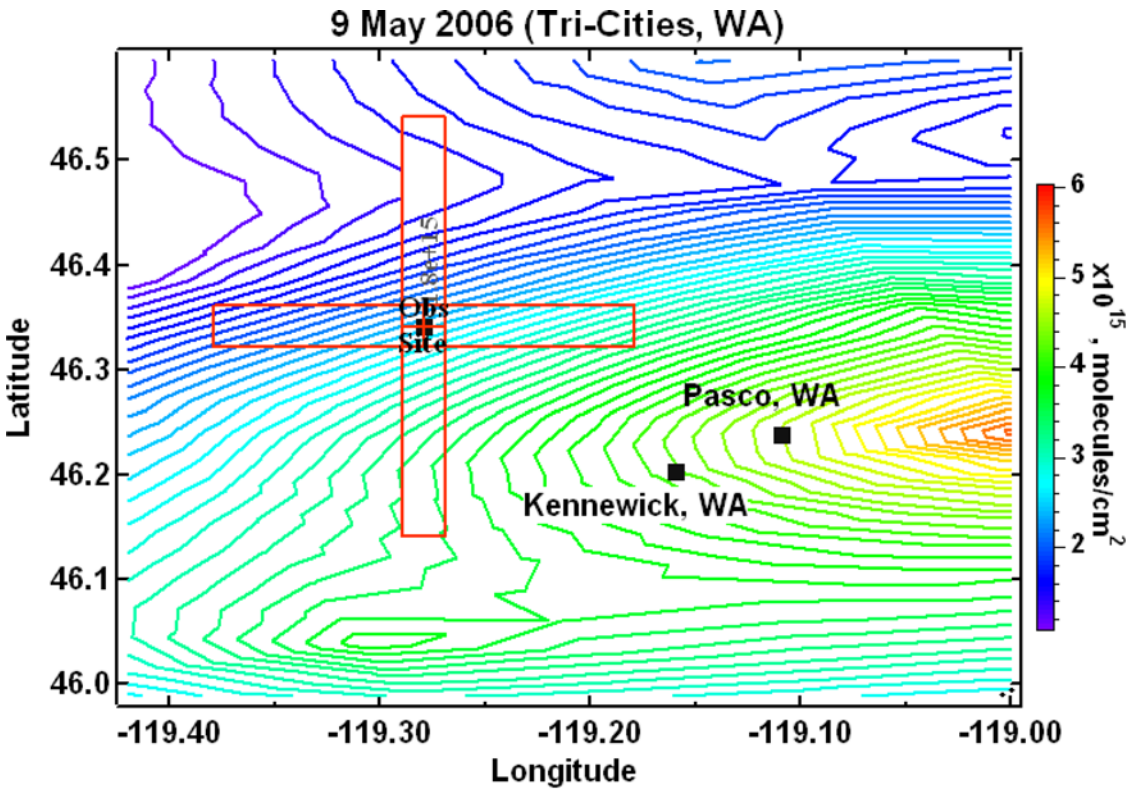

Figure 9. Tropospheric NO_2 VCD over the Tri-Cities area of Washington State on 9 May 2006. The contour map is derived from the individual OMI FOV measurements. The red rectangles show the tropospheric region viewed by the MF-DOAS instrument and reported in Figure 8 and are centered on the PNNL site. The centers of population for the cities of Kennewick and Pasco are indicated with black squares.

400–440 nm window, using a fixed reference spectrum determined from Pandora-1 data obtained over an extended period of at least 2 weeks. To estimate the NO_2 amount in the reference spectrum, a bootstrap method, as described in *Cede et al.* [2006], was applied, on the assumption that a few measurements were obtained when there were low tropospheric NO_2 amounts (e.g., just after sunrise).

[73] Figure 14 shows Pandora-1 data during the SCOUT campaign in July 2006 at Thessaloniki, Greece. Excellent agreement is seen between the OMI and Pandora-1 measurements, with OMI underestimating Pandora-1 by ~15%, on average. However, the OMI overpass times generally occur just before or just after the midday maximum in NO_2 concentration; this limits the range of NO_2 concentration values explored in this comparison. A number of further field campaigns are planned, during which Pandora-1/OMI comparisons will be performed.

4.3.3. Direct Sun DOAS (BIRA)

[74] During the second DANDELIONS campaign, BIRA operated a direct-Sun DOAS instrument in addition to the MAX-DOAS instrument. The well-defined optical path and purely geometric air mass factor make this instrument equally sensitive to absorption along the whole optical path and provides NO_2 total columns with an accuracy on the order of 15%.

[75] The instrument is similar in concept to the MAX-DOAS: Inside the building, in a thermoregulated box, a grating spectrometer covering the UV-Vis region is coupled to a cooled CCD detector, connected by depolarizing fiber optic bundle to the external optical head. Outside, alongside the MAX-DOAS scanning telescope, a collimating tube is mounted on a BRUSAG commercial Sun-tracking system, which holds the fiber.

[76] The retrieval is also done using the DOAS approach: The ratios of the measured radiance spectra to a reference spectrum are analyzed with respect to a set of reference spectra, in the 425–450 nm window, including laboratory spectra of O_3, H_2O, O_2-O_2, the computed the Ring effect spectrum, and NO_2 cross-sections at two different temperatures. In contrast to the analysis of MAX-DOAS data, a fixed reference spectrum (measured on 15 September 2006) has been used for the whole time series. The NO_2 residual slant column amount included in this reference spectrum has been obtained by analyzing it with respect to the Kurucz solar atlas [*Kurucz et al.*, 1984], which was assumed to be free of NO_2 absorption. The Kurucz solar spectrum was convolved with a precisely measured instrument slit function to match the instrument's spectral resolution. On the basis of this analysis, total absolute slant columns could be derived from direct Sun measurements; these were transformed into total vertical columns using geometrical AMFs. The accuracy of this technique can thus be estimated changing the DOAS analysis settings (differences up to 10% in the slant column) and a further check on the total NO_2 column is performed by comparing it to the total column of the MAX-DOAS instrument, obtained adding

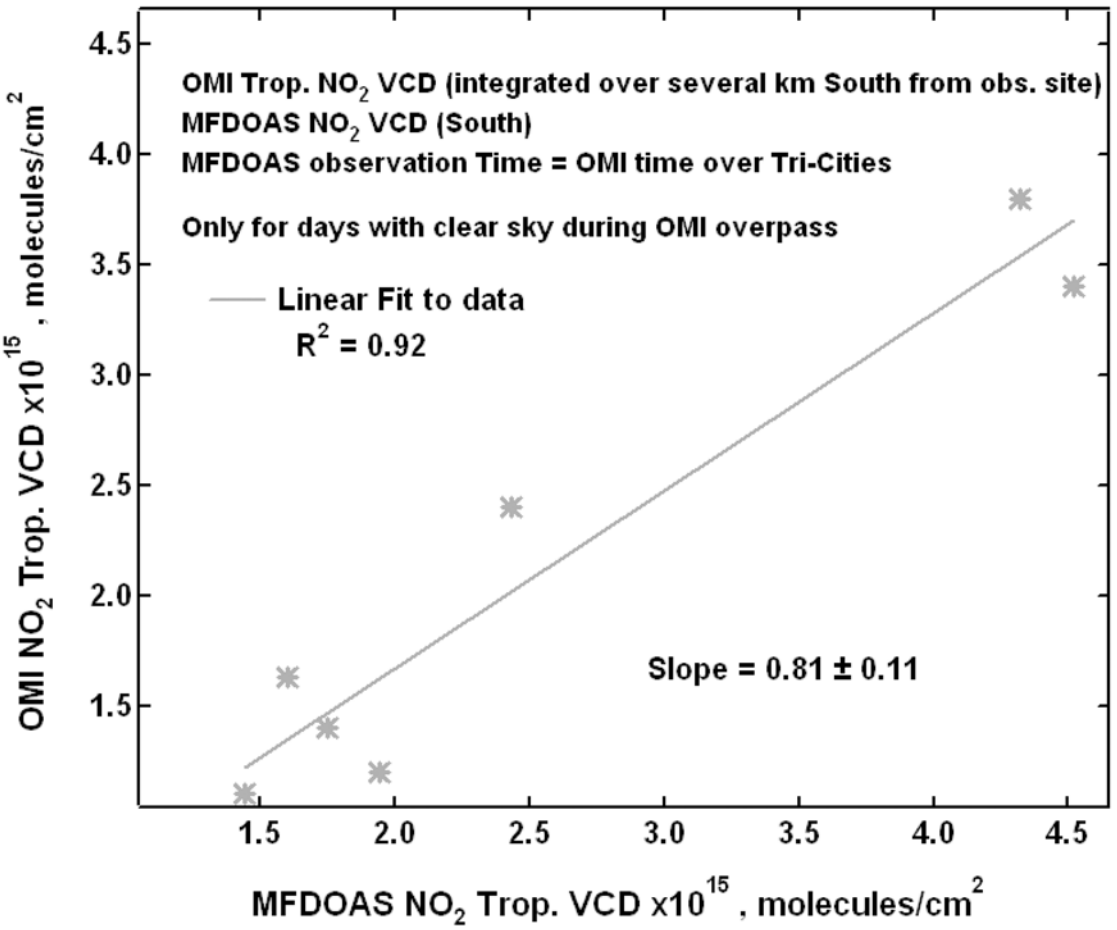

Figure 10. Correlation between OMI tropospheric NO_2 vertical column and MF-DOAS NO_2 tropospheric VCD for measurements made from 30 April through 13 May 2006. The points were equally weighted for the fit.

the tropospheric content to the estimated stratospheric amount. The agreement is within 15% for the reference day.

[77] Figure 15 shows the time series for the BIRA DOAS measurements of the total column NO_2 (filled dots), which provides a good idea of the diurnal variation of NO_2 levels. The open squares show the collocated OMI measurements (one or two per day). The OMI snapshots of vertical column NO_2, for the most part, appear to be in quite good agreement with the ground-based measurements. Note that the OMI data are filtered for clouds (cloud fraction $\leq$ 20%).

[78] Figure 16 shows the correlation plot of the collocated data (the point nearest in time to the OMI overpass). A linear regression, constrained to pass through the origin, gives a slope of 0.84 ± 0.05. The scatter in the data ($R = 0.68$) and the relatively small number of data points ($N = 26$) do not permit a statistically significant estimation of an additive bias.

4.3.4. FTUVS Measurements at Table Mountain, California

[79] Another instrument that has been used to validate OMI NO_2 total column measurements uses the Fourier Transform Ultraviolet Visible Spectrometer (FTUVS), a UV-VIS-NIR interferometer at the Table Mountain Facility (TMF) north of Los Angeles, California, at 34°22.9′N, 117°40.8′W at an altitude of 2290 m (7300′) [*Cageao et al.*, 2001]. Spectra are recorded in the direct solar absorption mode with a spectral resolution of 0.0013 nm, which is sufficient to resolve NO_2 vibronic features. By computing the ratio of the doppler-shifted spectra measured at the east and west solar limbs, one can remove the solar Fraunhofer lines; there is no need to measure a high-Sun reference spectrum, as in a number of the other methods described in this overview.

[80] The instrument is not readily transportable. The FTUVS observation site overlooks the Antelope Valley, north of the Los Angeles Basin. This area is characterized by relatively clean air under most conditions, but it is often influenced by polluted air from Los Angeles in the afternoon, advected through the Cajon Pass. While considerably above the tropospheric background under these conditions, the NO_2 column abundance values rarely exceed 1×10^{16} molecules cm^{-2}, which is considerably smaller than values measured directly downwind of a polluted urban area (see Figure 12). Because the altitude of TMF is about 2500 feet above the Antelope Valley, FTUVS column abundance measurements of NO_2 will be biased relative to the center of the OMI footprint. The bias is small relative to the total column and will not have a significant effect on the slope of the OMI-FTUVS correlation. The OMI data used for validation were

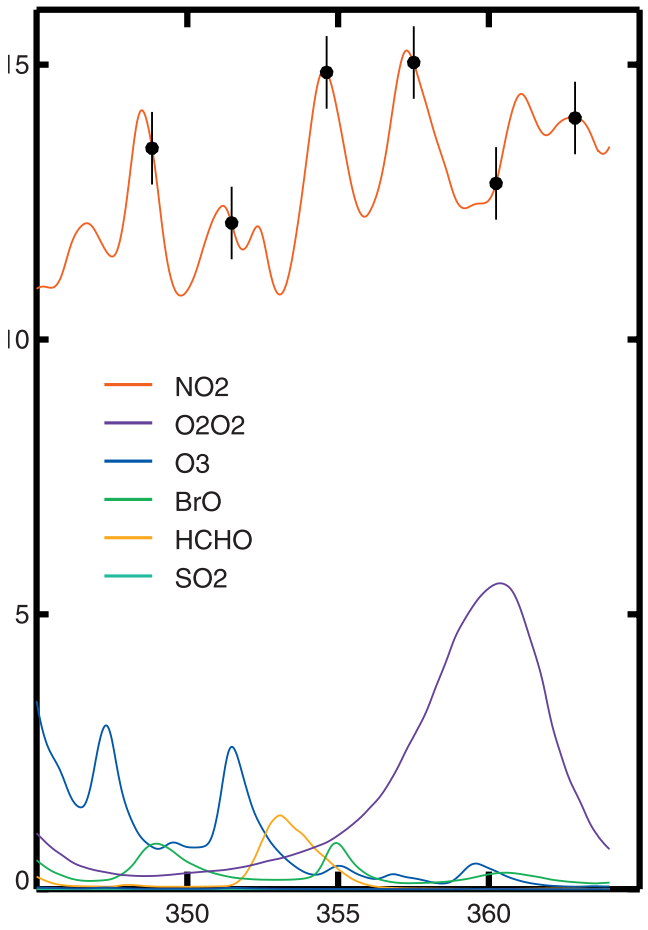

Figure 11. Typical optical depths of the main trace gases in the Brewer MK-III wavelength range. The red curve is the NO_2 optical thickness for 1 DU (= 2.7×10^{16} cm^{-2}), The black dots are placed on the red curve at the wavelengths of the six slit positions of the Brewer instrument. The vertical bars show the $\pm 2\sigma$ noise estimates for measurements at these wavelengths. The blue curve shows the optical thickness of a 315 DU column of ozone, and the purple curve shows the optical thickness of O_2-O_2 above a surface pressure of 1 atm. Other trace gases, at their typical concentrations (SO_2, HCHO, and BrO) have optical depths less than 2000 throughout this wavelength region.

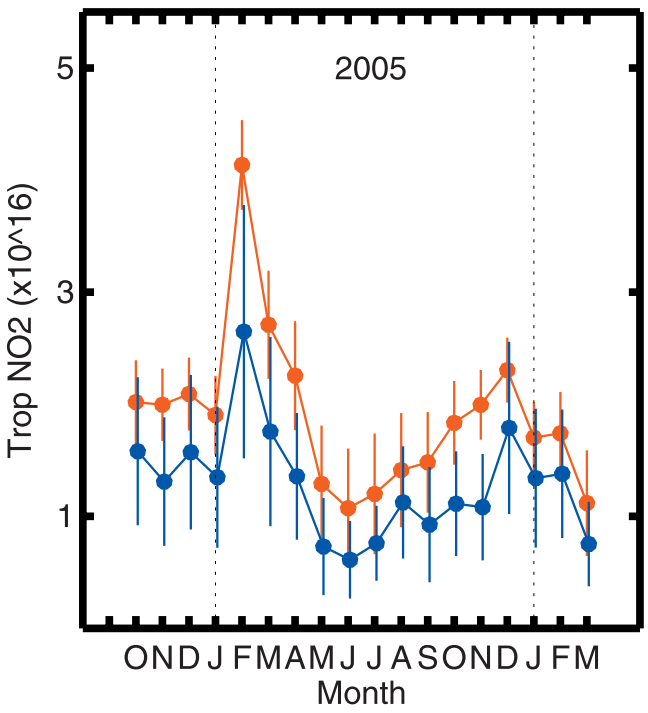

Figure 12. Comparison between the monthly mean Brewer-measured (red) and OMI-measured (blue) NO_2 total columns. The vertical bars show twice the standard errors.

sorted by distance from the TMF site, in order to mitigate the possible effects of the distribution of elevations within a FOV. It was found that a minimum distance of about 10 km is required for good intercomparison.

[81] The FTUVS instrument time is shared with other Aura validation activities. On average, measurements were acquired twice a week over the period March–November 2006.

[82] The slant column NO_2 amounts are retrieved by fitting the measured absorption spectra to laboratory spectra at a number of temperatures [*Nizkorodov et al.*, 2004] in windows containing 10 to 20 NO_2 rotational lines. Geometric AMFs were used to convert the SCDs to VCDs.

[83] Figure 17 presents the comparison of the OMI-derived and FTUVS-derived measurements of total column

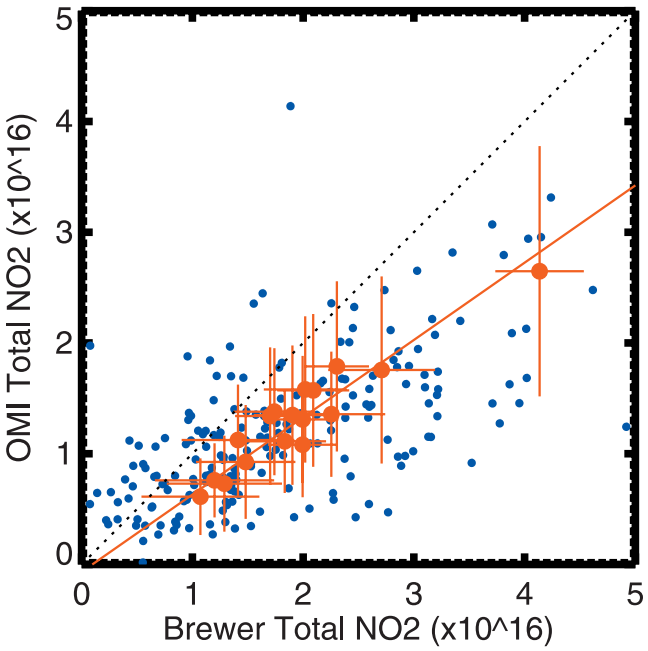

Figure 13. Daily mean (blue) and monthly mean (red) values of NO_2 total column measured by the Brewer instrument and OMI. The line of linear regression is also shown (slope = 0.70, intercept = -0.07×10^{16}). Horizontal and vertical bars on the monthly points show twice the standard errors of the respective quantities.

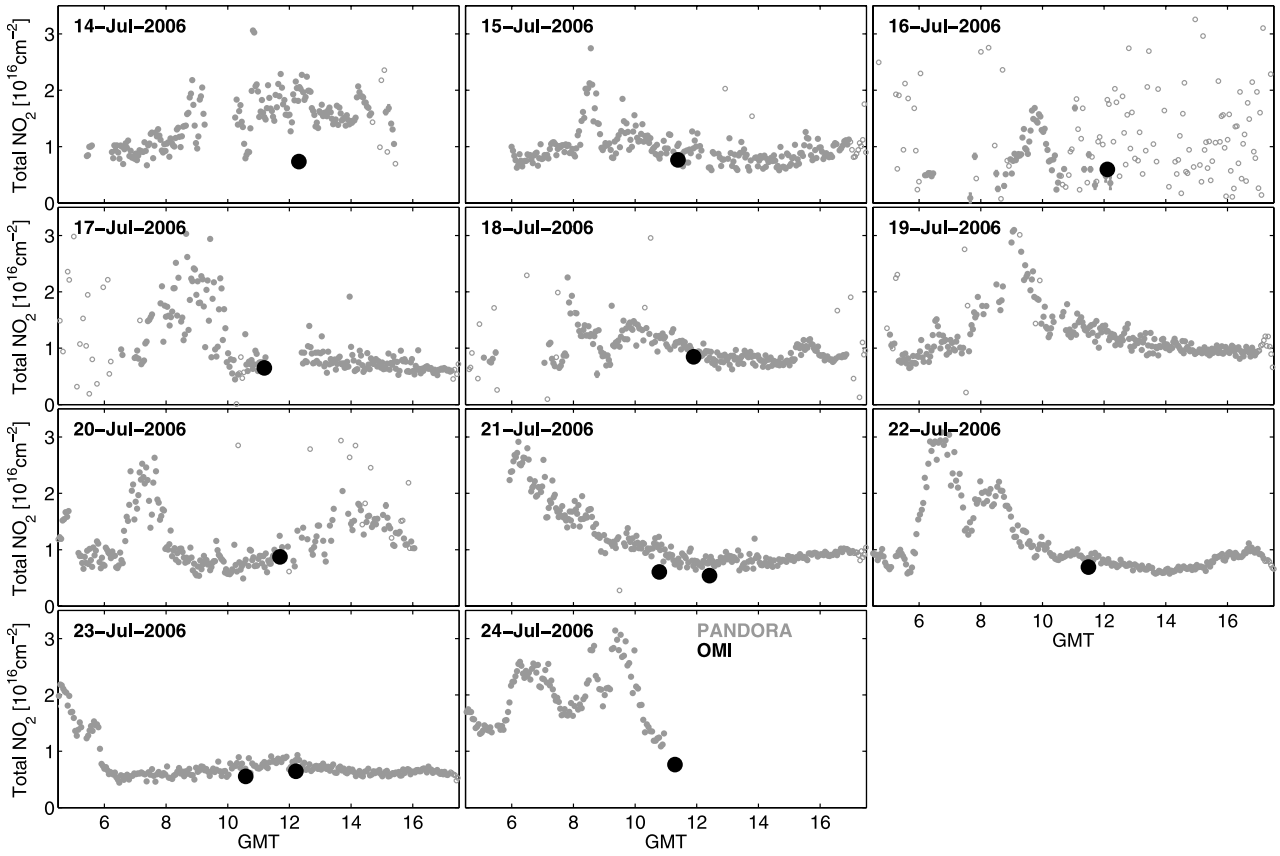

Figure 14. Pandora-1 data measured during the period 14–24 July 2006, in Thessaloniki (grey dots) and OMI overpass data for the site (large black dots).

NO_2. In this figure, the points where the OMI FOV center fell within 10 km of the Table Mountain Facility site are colored red. The linear regression line shown is fit only to those points. As shown, this line has a slope of 0.77 ± 0.41 and does not go through the origin. This data set suggests that the OMI NO_2 totals are underestimated in the middle of the data range but that there may also be a positive additive bias.

4.4. NO_2 Profile Measurements

[84] As pointed out in previous sections and in the work of *Boersma et al.* [2002] and *Bucsela et al.* [2006], the shape of the vertical profile of NO_2 influences the (physical)

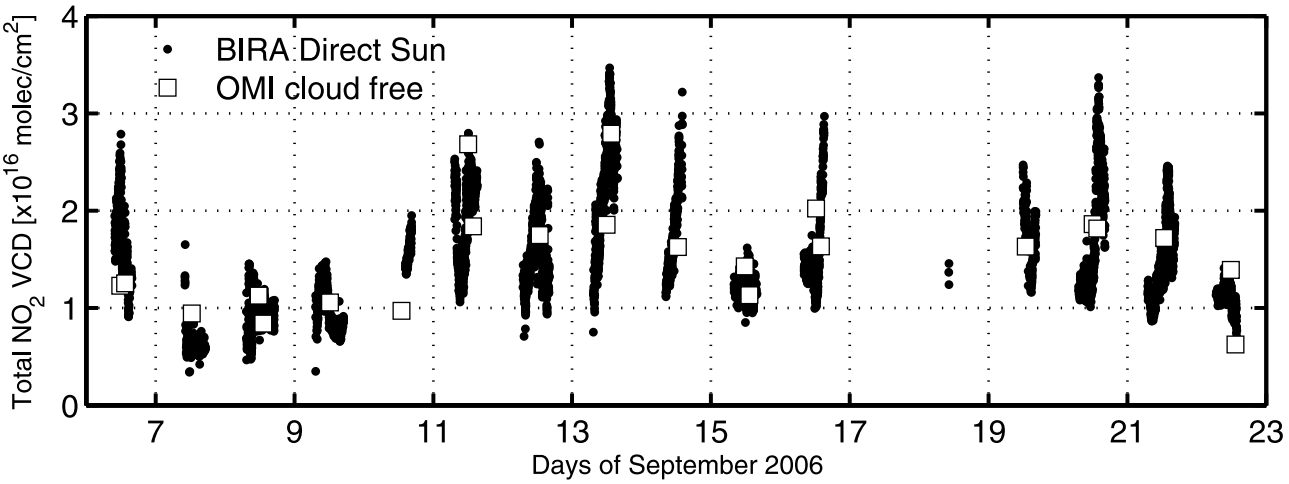

Figure 15. Time series of NO_2 VCD measured by the BIRA direct-Sun DOAS instrument. The open squares show the collocated OMI measurements.

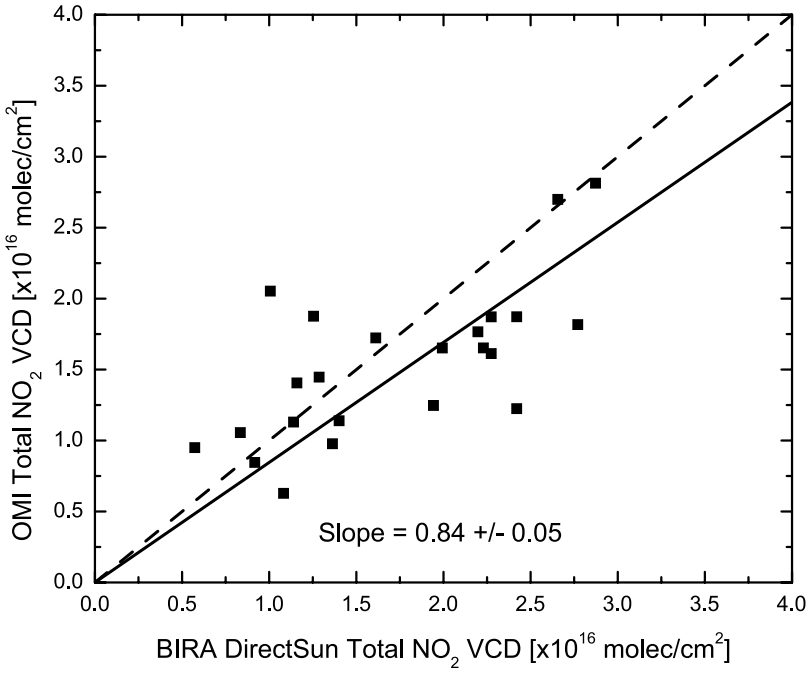

Figure 16. Correlation plot showing the collocated OMI and BIRA direct-Sun DOAS instrument measurements (open squares in Figure 15). The solid line is the regression fit and the dashed line is the 1:1 line.

air mass factors. The OMI NO_2 algorithm uses a set of assumed profiles, which were derived from model studies; these assumed profiles thus affect the retrieved total and tropospheric NO_2 amounts. It is therefore important to evaluate how large the influence of the assumed NO_2 profiles is on the retrieved NO_2. One way to assess this is to calculate air mass factors with true (measured) NO_2 profiles and compare these with the actual air mass factors used. However, there have been very few efforts to measure NO_2 profiles [*Heland et al.*, 2002; *Martin et al.*, 2006]. Recent efforts include measurements during the September 2006 DANDELIONS campaign (lidar, in situ at two alti-

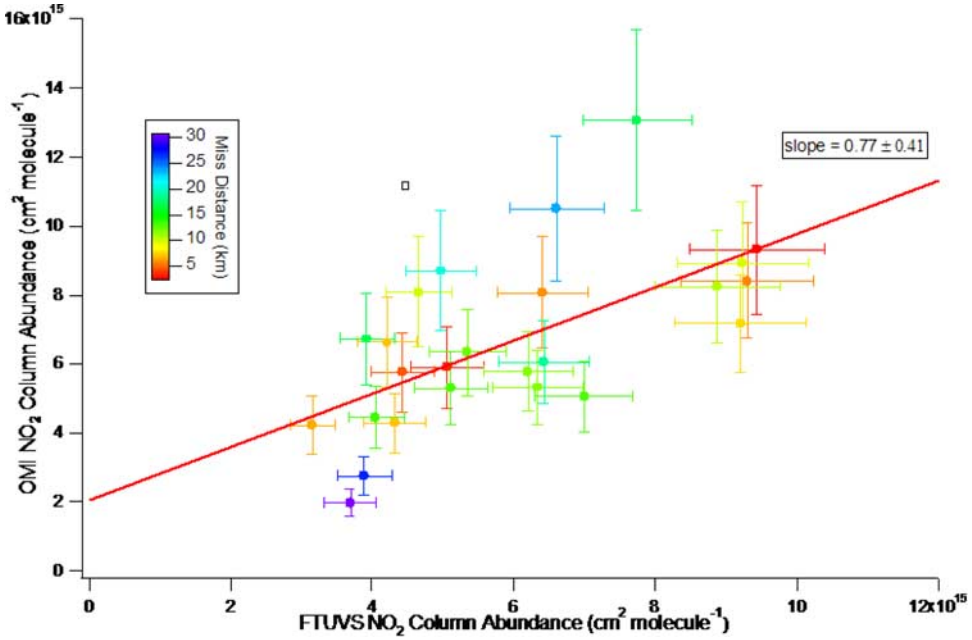

Figure 17. OMI versus FTUVS measurements of total column NO_2, binned by distance between TMF and the centroid of the OMI FOV (distance indicated by color, see inset scale). Error bars show the estimated 1σ uncertainty in the measurements.

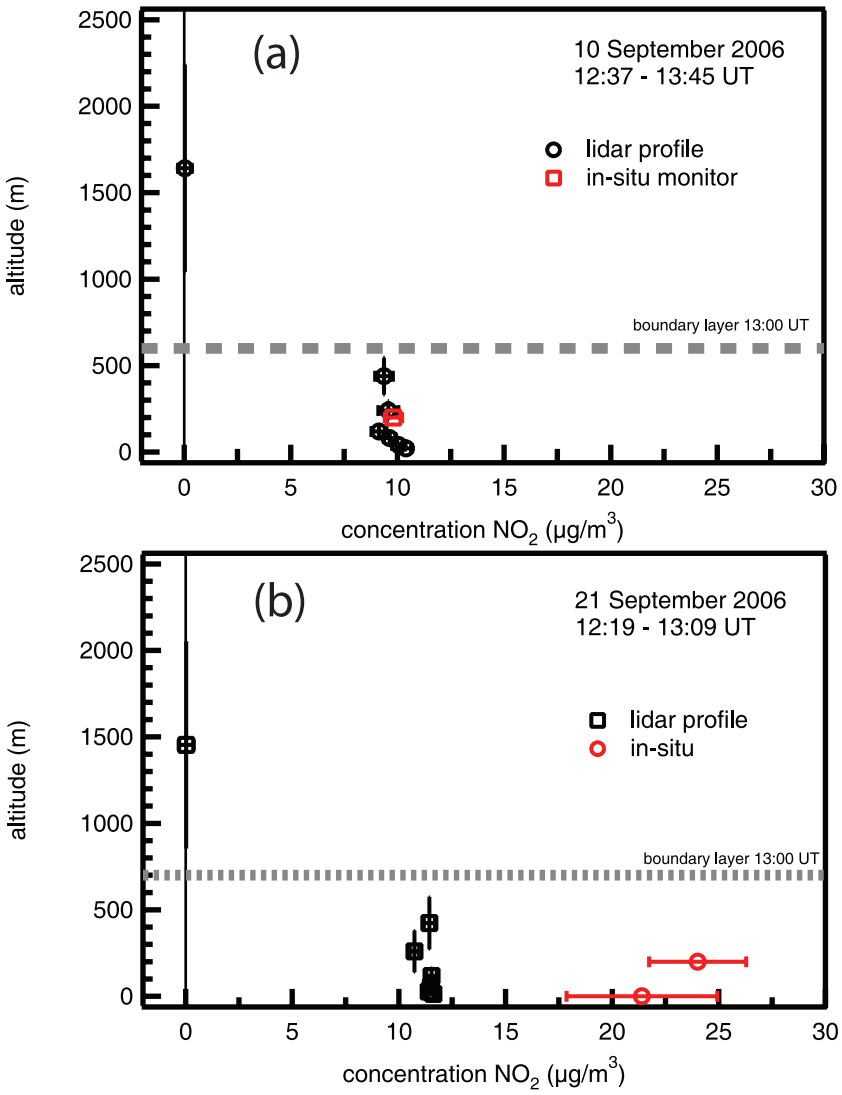

Figure 18. Lidar NO_2 profiles (black symbols) and NO_2 monitor values (red circles) measured at Cabauw. Horizontal bars indicate two-sigma uncertainties for the concentration. For the lidar data, vertical bars indicate the height intervals over which concentrations have been determined. The boundary layer height is indicated by a dashed line. (top) 10 September 2006. On this day, the NO_2 monitor at ground level was not operational. NO_2 monitor data at 200 m were averaged over the lidar integration time. (bottom) 21 September 2006.

tudes, and MAX-DOAS at two altitudes, see section 4.4.1), and aircraft-based in situ measurements taken during the INTEX-B campaign in North America.

4.4.1. Comparison of NO_2 Lidar With in Situ and OMI Data

[85] Figure 18 presents examples of lidar profiles on two similarly polluted days, 10 September 2006 and 21 September 2006; in both cases there was little to no cloud cover. Profile measurements take about 50 min and are timed to coincide with an OMI (or SCHIAMACHY) overpass. These measurements illustrate the general observation that the concentration of NO_2 is higher at ground level and drops nearly to zero (below the lidar detection limit) above the boundary layer. The boundary layer heights, provided by the boundary layer lidar at Cabauw, are indicated in Figure 18 by dashed lines. During the dandelions campaign we found large diurnal and day-to-day variations in NO_2 at the surface, from around 3 μg m^{-3}, on a clean day, to more than 50 μg m^{-3} on a polluted day. The red symbols in Figure 18 show the corresponding in situ monitor data. For 10 September, only data of the NO_2 monitor located at 200 m was obtained. The NO_2 monitor data, sampled once per minute, are averaged over the 50 min lidar integration. On 10 September there is excellent agreement between the NO_2 monitor data point and the lidar-profile data points. On 21 September, the discrepancy between the lidar-derived NO_2 concentrations and the in situ data is considerable.

[86] We can make a provisional comparison with OMI Level-2 vertical column densities if we average the lidar concentration measurements and use this value as a constant NO_2 concentration located within the boundary

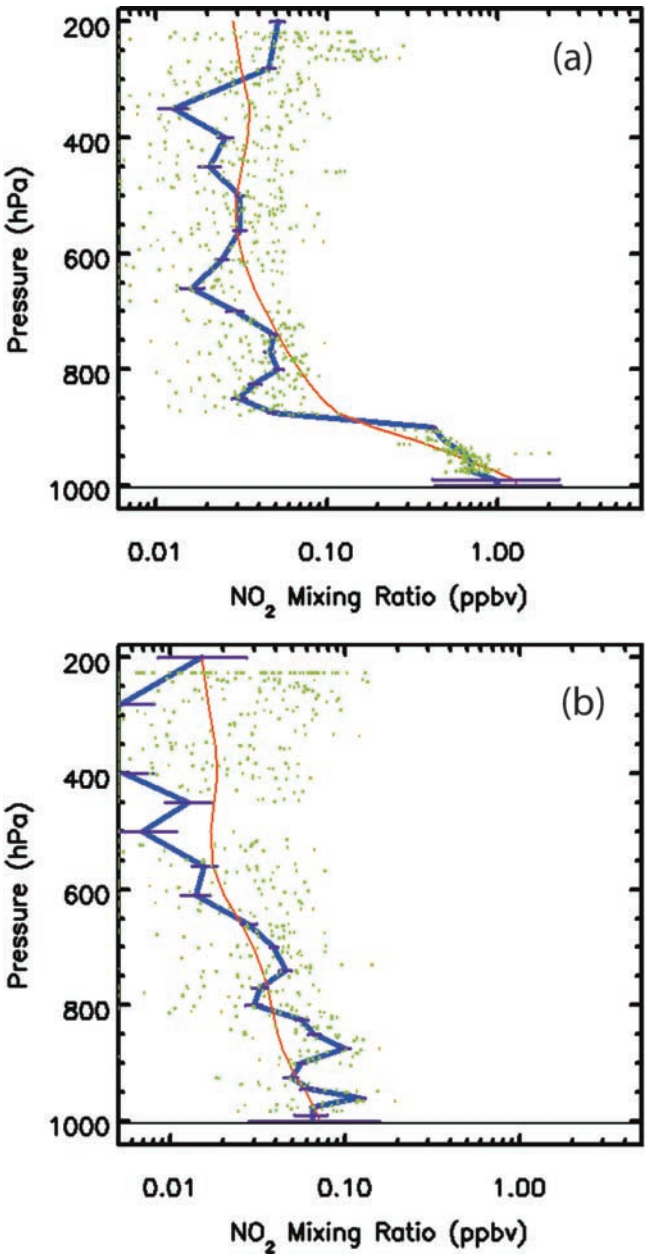

Figure 19. Two INTEX-B NO_2 profiles showing (top) data for a profile measured over the Mississippi-Alabama border (33.2 N, 88.3 W) and (bottom) data for a profile measured over the Gulf of Mexico (23.0 N, 91.1 W). Green dots are original measurements, the blue line is the binned profile, and the red line is the annual mean GEOS-CHEM model profile for that location.

layer. For 10 September the OMI tropospheric VCD was 6.7×10^{15} cm^{-2}. This agrees well with the derived lidar VCD of $(7.5 \pm 1.0) \times 10^{15}$ cm^{-2}. The agreement on 21 September was poorer: The OMI VCD was 14.7×10^{15} cm^{-2}, whereas the derived lidar VCD was $(10.3 \pm 1.0) \times 10^{15}$ cm^{-2}. If we derive a VCD using a constant averaged in situ monitor value located within the boundary layer, we obtain a value of $(21 \pm 2) \times 10^{15}$ cm^{-2}, which is much higher than either the lidar or OMI VCD.

[87] To understand the discrepancies between lidar, in situ, and OMI data, a more detailed study is necessary (H. Volten et al., manuscript in preparation, 2008). An important candidate to explain the discrepancies is the spatial heterogeneity of the NO_2 field (see also section 4.2.3). Additional lidar measurements taken during the dandelions campaign show that NO_2 concentrations obtained for the same time interval but for different horizontal directions may easily differ by four or five μg m^{-3}. Another possible explanation for the relatively high OMI data may be that we incorrectly assume that all the NO_2 is located in the boundary layer. Model calculations show that up to about 20% of the NO_2 may be located in the free troposphere [*Blond et al.*, 2007]. For the in situ data, interference from NH_3 may account for overestimates in NO_2 of up to 6%.

4.4.2. In Situ Aircraft Measurements

[88] In situ measurements of NO_2 from the DC-8 aircraft were obtained during the INTEX-A (summer 2004), PAVE (winter 2005), and INTEX-B (spring 2006) campaigns. These have been discussed by *Bucsela et al.* [2008]. The NO_2 profiles from these experiments are useful for validating both the shapes of the model profiles used in the OMI retrieval algorithm, and, in turn, the tropospheric column amounts from the satellite retrievals. The aircraft profiles obtained during INTEX-A and PAVE were combined into composite land and ocean profiles. The in situ profiles were seen to be very similar to the annual mean GEOS-CHEM profiles used to retrieve tropospheric NO_2 columns from OMI, and the AMFs computed from the measured profiles were slightly larger than those calculated using the model profiles. A more quantitative analysis was performed using a set of approximately 70 profiles measured during INTEX-B. Error-weighted linear regressions comparing the AMFs from modeled and measured profiles yielded a slope of 1.10 $\pm$ 0.10 (in situ profile AMF greater than that used by the OMI algorithm). This means that the OMI VCD would overestimate the actual VCD by 10% $\pm$ 10%, based on the profile shape alone.

[89] In situ measurements of NO_2 can also be used to validate tropospheric column amounts from OMI. The INTEX-B data were used for this analysis by *Bucsela et al.* [2008] (see also *Boersma et al.* [2008]). Two representative profile analyses are shown in Figure 19. The full set of profiles from INTEX-B were used; the correlation between the aircraft and OMI data sets was good (R = 0.83). This comparison is shown in Figure 20. The OMI Level-2 columns were found to be somewhat smaller than the integrated in situ profiles, as indicated by the slope of 0.86 ± 0.11. Clearly, the influence of the AMF, as discussed just above, is outweighed by other effects. Although some of the in situ columns required significant extrapolations, sensitivity studies indicated that the overall results were generally robust with respect to the choices made for the profile binning, integration and extrapolation, as well as being relatively insensitive to the errors assumed for the weights. The insensitivity to extrapolation is consistent with findings in a similar aircraft study by *Heland et al.* [2002].

5. Conclusions and Discussion

[90] This paper has presented a number of results of experiments where ground- and aircraft-based measure-

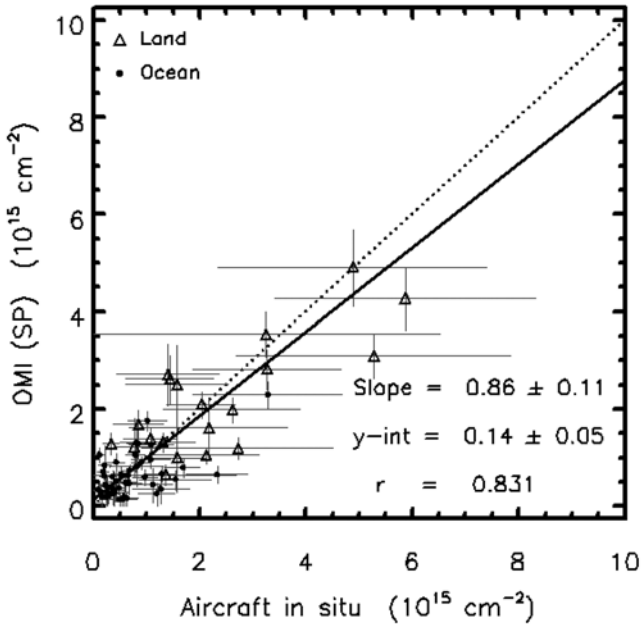

Figure 20. OMI tropospheric NO_2 columns as a function of integrated aircraft in situ measurements from INTEX-B. The symbols indicate land measurements (triangle) or ocean measurements (dot). The error bars show the estimated uncertainties in both variables. The dotted line is a 1:1 ratio and the solid line is the fit to the data.

ments of NO_2 can be compared with collocated measurements and retrievals by OMI. Since some measurements estimate the stratospheric column, others estimate the tropospheric column, and still others estimate the total column, their results can be used to validate the OMI NO_2 standard data product's estimates of these columns. Table 3 summarizes the results of the numerous validation studies that have been discussed in this overview.

[91] On the basis of the SAOZ and DOAS measurements, which are most sensitive to the stratospheric NO_2 columns, the OMI stratospheric NO_2 appears to have a negative bias with respect to the ground-based measurements by an average of ~14%. However, occasionally the disagreement can be as great as 20% in the tropics, where the small stratospheric column means that small absolute differences correspond to large relative differences.

[92] The OMI tropospheric column appears to be consistently smaller than the various ground-based measurements, though there is some inconsistency amongst those ground-based measurements. Although many of the various instruments and methods for measuring tropospheric and total NO_2 have not themselves been validated, it is noteworthy that they all give NO_2 estimates that are on average greater than those retrieved from OMI. This may indicate a bias in the OMI retrieval. However, a number of cases have been studied where average differences between OMI and ground-based measurements decrease as the geographic match up criterion is tightened. This is likely to be due to the inhomogeneity of the tropospheric NO_2 field, and, in particular, the fact that ground-based measurements are often made in or near regions of moderate to strong sources of NO_2: The OMI FOV that includes the site also includes a substantial ($\sim 10^2$ km^2) region where much lower NO_2 concentrations prevail. This was borne out in the Brewer studies [*Cede et al.*, 2006] and in the correlation studies of J. P. Veefkind (private communication, 2007) (see also section 1.) The data taken at TMF (section 4.3.4) were mostly obtained under conditions of relatively clean tropospheric air, and these data also suggested a negative bias for OMI retrieved total NO_2.

[93] We have also mentioned that a small number of aircraft in situ measurements of NO_2 suggest that OMI underestimates the tropospheric column by about 15%. The uncertainties in these measurements, however, are large due to the scatter of the in situ data (with both random and systematic errors possible), and the fact that the aircraft does not sample the entire troposphere (systematic bias).

[94] Potential biases can arise at any of the steps in the algorithm. Instrumental artifacts are known to give rise to the cross-track bias (striping) and the destriping process can certainly give rise to a general bias. The stratosphere-troposphere separation is based on an initial AMF, and any bias in that AMF will result in a bias in the background (mostly stratospheric) field. After the stratosphere-troposphere separation, a new AMF is constructed, based on model-based-climatology derived a priori profiles. The aircraft in situ measurements of NO_2 profile shape suggest that the a priori profile shapes are essentially correct, in that the two do not give appreciably different AMFs. Further, the AMF is quite sensitive to the surface albedo. The OMI algorithm uses a climatological surface albedo that was derived from GOME measurements [*Koelemeijer et al.*, 2003]. While the values are generally reasonable, some outliers have been identified, and the values have not been validated.

[95] The effects of aerosols on retrievals, and most of the ground-based measurements, have not been investigated. It is possible that aerosols can mask some of the tropospheric NO_2, hence introducing a low bias in the retrieved columns. A bias in OMI NO_2 due to aerosols would generally not be

Table 3. Summary of Validation Study Results for OMI NO_2 Data Product

Instrument	Column	Group	OMI, Relative to GB	Uncertainty	Remarks
SAOZ	stratospheric	CNRS	−14%	±10%	as large as 25% in tropics
MAX-DOAS	tropospheric	BIRA, etc.	−15%	—	large scatter in the data
MF-DOAS	tropospheric	WSU	−19%	±11%	very small *N*
Aircraft in situ	tropospheric	UC, GSFC	−15%	±10%	large scatter
Brewer	total	GSFC	−33%	—	large *N*, large scatter
Pandora-1	total	GSFC	−15%	—	very small *N*, small data range
DS-DOAS	total	BIRA	−16%	±5%	small *N*, large scatter
FTUVS	total	JPL	−23%	±41%	small *N*, significant apparent bias but good correlation

identical to the bias in ground-based measurements; the bias of OMI relative to ground-based may be either positive or negative.

[96] It should be mentioned that all the validation studies reviewed here focused on mostly cloud-free conditions. However, while OMI FOVs are considerably smaller than those of earlier atmospheric remote sensing instruments, they are still large enough that very few can be expected to be completely uncontaminated by clouds.

[97] **Acknowledgments.** Part of this research was carried out at the Jet Propulsion Laboratory, California Institute of Technology, under contract with the National Aeronautics and Space Administration. The DANDELIONS campaigns were supported in part by grants from ACCENT-Troposat.

References

Bey, I., D. J. Jacob, R. M. Yantosca, J. A. Logan, B. D. Field, A. M. Fiore, Q. Li, H. Y. Liu, L. J. Mickley, and M. G. Schultz (2001), Global modeling of tropospheric chemistry with assimilated meteorology: Model description and evaluation, *J. Geophys. Res.*, *106*, 23,073–23,096.

Blond, N., K. F. Boersma, H. J. Eskes, R. J. van der A, M. van Roozendael, I. De Smedt, G. Bergametti, and R. Vautard (2007), Intercomparison of SCIAMACHY nitrogen dioxide observations, in situ measurements and air quality modeling results over Western Europe, *J. Geophys. Res.*, *112*, D10311, doi:10.1029/2006JD007277.

Boersma, K. F., E. Bucsela, E. Brinksma, and J. F. Gleason (2002), NO_2, in *OMI Algorithm Theoretical Basis Document*, vol. IV, *Trace Gas Algorithms*, edited by K. Chance, pp. 15–36, NASA Goddard Space Flight Cent., Greenbelt, Md.

Boersma, K. F., H. J. Eskes, and E. J. Brinksma (2004), Error analysis for tropospheric NO_2 retrieval from space, *J. Geophys. Res.*, *109*, D04311, doi:10.1029/2003JD003962.

Boersma, K. F., et al. (2008), Validation of OMI tropospheric NO_2 observations during INTEX-B and application to constrain NOx emissions over the eastern United States and Mexico, *Atmos. Environ.*, doi:10.1016/j.atmosenv.2008.02.004, in press.

Bovensmann, H., J. P. Burrows, M. Buchwitz, J. Frerick, V. V. Rozanov, K. V. Chance, and A. P. H. Goede (1999), SCIAMACHY: Mission objectives and measurement modes, *J. Atmos. Sci.*, *56*, 127–150.

Brinksma, E. J., et al. (2008), The 2005 and 2006 DANDELIONS NO_2 and aerosol intercomparison campaigns, *J. Geophys. Res.*, doi:10.1029/2007JD008808, in press.

Bucsela, E., et al. (2008), Comparison of tropospheric NO_2 from in situ aircraft measurements with near-real time and standard product data from the Ozone Monitoring Instrument, *J. Geophys. Res.*, doi:10.1029/2007JD008838, in press.

Bucsela, E. J., E. A. Celarier, M. O. Wenig, J. F. Gleason, J. P. Veefkind, K. F. Booersma, and E. J. Brinksma (2006), Algorithm for NO_2 vertical column retrieval from the Ozone Monitoring Instrument, *IEEE Trans. Geosci. Remote Sens.*, *44*(5), 1245–1258, doi:10.1109/TGRS.2005.863715.

Burrows, J. P., A. Richter, A. Dehn, B. Deters, S. Himmelmann, S. Voigt, and J. Orphal (1999a), Atmospheric remote sensing reference data from GOME-2. temperature-dependent absorption cross-sections of O_3 in the 231–794 nm range, *J. Quant. Spectrosc. Radiat. Transfer*, *61*, 509–517.

Burrows, J. P., M. Weber, M. Buchwitz, V. V. Rozanov, A. Ladstatter-Weissenmayer, A. Richter, R. DeBeek, R. Hoogen, K. Bramstedt, and K. U. Eichmann (1999b), The global ozone monitoring experiment (GOME): Mission concept and first scientific results, *J. Atmos. Sci.*, *56*, 151–175.

Cageao, R. P., J. F. Blavier, J. P. McGuire, Y. B. Jiang, V. Nemtchinov, F. P. Mills, and S. P. Sander (2001), High resolution fourier transform ultraviolet-visible spectrometer for the measurement of atmospheric trace species: Application to OH, *Appl. Opt.*, *40*, 2024–2030.

Cede, A., J. Herman, A. Richter, N. Krotkov, and J. Burrows (2006), Measurements of nitrogen dioxide total column amounts using a Brewer double spectrophotometer in direct sun mode, *J. Geophys. Res.*, *111*, D05304, doi:10.1029/2005JD006585.

Celarier, E. A., J. F. Gleason, E. J. Bucsela, K. F. Boersma, E. Brinksma, J. P. Veefkind, and P. Levelt (2006), OMNO2 README file, technical report, NASA Goddard Space Flight Cent., Greenbelt, Md. (Available at http://toms.gsfc.nasa.gov/omi/no2/OMNO2_readme.pdf.)

Chance, K. V., and R. J. D. Spurr (1997), Ring effect studies: Rayleigh scattering, including molecular parameters for rotational Raman scattering, and the Fraunhofer spectrum, *Appl. Opt.*, *36*(21), 5224–5230.

Cleary, P. A., P. J. Wooldridge, and R. C. Cohen (2002), Laser-induced fluorescence detection of atmospheric NO_2 with a commercial diode laser and a supersonic expansion, *Appl. Opt.*, *41*, 6950–6956.

Denis, L., H. K. Roscoe, M. P. Chiperfield, M. van Roosendael, and F. Goutail (2005), A new software suite for NO_2 vertical profile retrieval from ground-based zenith-sky spectrometers, *J. Quant. Spectrosc. Radiat. Transfer*, *92*(3), 321–333.

Deutschmann, T., and T. Wagner (2006), *TRACY-II Users Manual*, Univ. of Heidelberg, Heidelberg, Germany.

Dobber, M., et al. (2006), Ozone monitoring instrument calibration, *IEEE Trans. Geosci. Rem. Sens.*, *44*(5), 1209–1238, doi:10.1109/TGRS.2006.869987.

Finlayson-Pitts, B. J., and J. Pitts (2000), *Chemistry of the Upper and Lower Atmosphere: Theory, Experiments, and Applications*, Elsevier, New York.

Gordley, L., et al. (1996), Validation of nitric oxide and nitrogen dioxide measurements made by the halogen occultation experiment for UARS platform, *J. Geophys. Res.*, *101*(D6), 10,241–10,266, doi:A1996UJ40400034.

Heland, J., H. Schlager, A. Richter, and J. P. Burrows (2002), First comparison of tropospheric NO_2 column densities retrieved from GOME measurements and in situ aircraft profile measurements, *Geophys. Res. Lett.*, *29*(20), 1983, doi:10.1029/2002GL015528.

Ionov, D., F. Goutail, and J. Pommereau (2006a), Validation of satellite data on total NO_2: GOME, SCIAMACHY and OMI nadir viewing instruments compared to UV-visible SAOZ network, paper presented at 3rd International DOAS Workshop, Inst. of Environ. Phys., Univ. of Bremen, Bremen, Germany, 20–22 March.

Ionov, D., F. Goutail, J.-P. Pommereau, A. Bazureau, E. Kyro, T. Portafaix, G. Held, P. Ericksen, and V. Dorokhov (2006b), Ten years of NO_2 comparisons between ground-based SAOZ and satellite instruments (GOME, SCIAMACHY, OMI), in *Atmospheric Science Conference, ESRIN, Frascati, Italy, 8–12 May 2006*, edited by D. Dansey, *Eur. Space Agency Spec. Publ., ESA SP-628*.

Ionov, D., Y. Timofeyev, F. Goutail, J.-P. Pommereau, and A. Shalamyansky (2007), Delta-validation of ENVISAT SCIAMACHY total ozone and NO_2 with the data of ground-based UV-VIS measurements (M-124 and SAOZ), in *3rd Workshop on the Atmospheric Chemistry Validation of Envisat (ACVE-3), ESRIN, Italy, 4–7 December 2006*, edited by H. Lacoste, *Eur. Space Agency Spec. Publ., ESA SP-642*.

Koelemeijer, R. B. A., J. F. de Haan, and P. Stammes (2003), A database of spectral surface reflectivity in the range 335–772 nm derived from 5.5 years of GOME observations, *J. Geophys. Res.*, *108*(D2), 4070, doi:10.1029/2002JD002429.

Kurucz, R. L., I. Furenlid, J. Brault, and L. Testerman (1984), *Solar Flux Atlas From 296 nm to 1300 nm: National Solar Observatory Atlas No. 1*, Natl. Sol. Obs., Sunspot, N. M.

Lambert, J., et al. (2001), Combined characterisation of GOME and TOMS total ozone measurements from space using ground-based observations from the NDSC, *Adv. Space Res.*, *26*(12), 1931–1940.

Levelt, P. F., E. Hilsenrath, G. W. Leppelmeier, G. H. J. van den Oord, P. K. Bhartia, J. Tamminen, J. F. de Haan, and J. P. Veefkind (2006a), Science objectives of the Ozone Monitoring Instrument, *IEEE Trans. Geosci. Remote Sens.*, *44*(5), 1199–1208, doi:10.1109/TGRS.2006.872336.

Levelt, P. F., G. H. J. van den Oord, M. R. Dobber, A. Malkki, H. Visser, J. de Vries, P. Stammes, J. Lundell, and H. Saari (2006b), The Ozone Monitoring Instrument, *IEEE Trans. Geosci. Remote Sens.*, *44*(5), 1093–1101, doi:10.1109/TGRS.2006.872333.

Martin, R., C. Sioris, K. Chance, T. Ryerson, T. Bertram, P. Woolridge, R. Cohen, J. Neuman, A. Swanson, and F. Flocke (2006), Evaluation of space-based constraints on nitrogen oxide emissions with regional aircraft measurements over and downwind of eastern North America, *J. Geophys. Res.*, *111*, D15308, doi:10.1029/2005JD006680.

Martin, R. V., et al. (2002), Interpretation of TOMS observations of tropical tropospheric ozone with a global model and in situ observations, *J. Geophys. Res.*, *107*(D18), 4351, doi:10.1029/2001JD001480.

Nizkorodov, S. A., S. P. Sander, and L. R. Brown (2004), Temperature and pressure dependence of high-resolution air-broadened absorption cross sections of NO_2 (415–525 nm), *J. Phys. Chem.*, *A108*, 4864–4872.

Noxon, J. F. (1975), Nitrogen-dioxide in stratosphere and troposphere measured by ground-based absorption spectroscopy, *Science*, *189*, 547–549.

Piters, A., K. Bramstedt, J. Lambert, and B. Kirchhoff (2006), Overview of SCHIAMACHY validation: 2002–2004, *Atmos. Chem. Phys.*, *6*, 127–148.

Platt, U. (1994), *Differential Optical Absorption Spectroscopy (DOAS), Air Monitoring by Spectroscopic Techniques*, vol. 127, *Chem. Anal. Ser.*, John Wiley, Hoboken, N. J.

Russchenberg, H., et al. (2005), Groundbased atmospheric remote sensing in The Netherlands; European outlook, *IEICE Trans. Commun., E88-B*, (6), 2252–2258, doi:10.1093/ietcom/e88-b.6.2252.

Spurr, R. J. D. (2001), Linearized radiative transfer theory: A general discrete ordinate approach to the calculation of radiances and analytic weighting functions, with application to atmospheric remote sensing, Ph.D. thesis, Tech. Univ. of Eindhoven, Eindhoven, Netherlands.

Spurr, R. J. D., T. P. Kurosu, and K. V. Chance (2001b), A linearized discrete ordinate radiative transfer model for atmospheric remote sensing retrieval, *J. Quant. Spectrosc. Radiat. Transfer*, *68*, 689–735.

Thornton, J. A., P. J. Wooldridge, and R. C. Cohen (2000), Atmospheric NO_2: In situ laser-induced fluorescence detection at parts per trillion mixing ratios, *Anal. Chem.*, *72*, 528–539.

Vandaele, A. C., C. Hermans, P. C. Simon, M. Carleer, R. Colin, S. Fally, M. F. Mérienne, A. Jenouvrier, and B. Coquart (1998), Measurements of the NO_2 absorption cross-section from 42000 cm^{-1} to 10000 cm^{-1} (238–1000 nm) at 220 K and 294 K, *J. Quant. Spectrosc. Radiat. Transfer*, *59*, 171–184.

Veefkind, J. P. and E. A. Celarier (2006), OMI Level 2 NO_2 data product specification, *Tech. Rep. SD-OMIE-KNMI-352*, NASA Goddard Space Flight Cent., Greenbelt, Md. (Available at http://disc.sci.gsfc.nasa.gov/Aura/OMI/OMNO2_data_product_specification.pdf.)

Wagner, T., B. Dix, C. v. Friedeburg, U. Frieß, S. Sanghavi, R. Sinreich, and U. Platt (2004), MAX-DOAS O4 measurements - A new technique to derive information on atmospheric aerosols. (I) Principles and information content, *J. Geophys. Res.*, *109*, D22205, doi:10.1029/2004JD004904.

Wagner, T., et al. (2007), Comparison of box-air-mass-factors and radiances for Multiple-Axis Differential Optical Absorption Spectroscopy (MAX-DOAS) Geometries calculated from different UV/visible radiative transfer models, *Atmos. Chem. Phys*, *7*, 1809–1833.

Wenig, M. O., A. M. Cede, E. J. Bucsela, E. A. Celarier, K. F. Boersma, J. P. Veefkind, E. Brinksma, J. F. Gleason, and J. R. Herman (2008), Validation of OMI tropospheric NO_2 column densities using direct-Sun mode Brewer measurements at NASA Goddard Space Flight Center, *J. Geophys. Res.*, doi:10.1029/2007JD008988, in press.

Wittrock, F., H. Oetjen, A. Richter, S. Fietkau, T. Medeke, A. Rozanov, and J. P. Burrows (2004), MAX-DOAS measurements of atmospheric trace gases in Ny-Ålesund - Radiative transfer studies and their application, *Atmos. Chem. Phys.*, *4*, 955–966.

B. Bojkov, E. J. Bucsela, A. Cede, and M. O. Wenig, GEST Program, University of Maryland, Baltimore County, Baltimore, MD 21250, USA.

E. Brinksma, M. Kroon, P. F. Levelt, J. P. Veefkind, and H. Volten, Royal Netherlands Meteorological Institute, NL-3730 AE De Bilt, Netherlands. (ellen.brinksma@knmi.nl)

E. A. Celarier, SGT, Inc., 7701 Greenbelt Road, Greenbelt, MD 20770, USA. (edward.celarier@gsfc.nasa.gov)

C. M. Chen, T. J. Pongetti, and S. P. Sander, Science Division, NASA Jet Propulsion Laboratory, California Institute of Technology, Pasadena, CA 91109, USA.

J. F. Gleason and J. R. Herman, NASA Goddard Space Flight Center, Code 613.3, Greenbelt, MD 20771, USA.

F. Goutail, and J.-P. Pommereau, CNRS, Route des Gatines, F-91370 Verrières le Buisson, France.

O. W. Ibrahim Institute for Environmental Physics, University of Heidelberg, D-69120 Heidelberg, Germany.

D. Ionov, Department of Atmospheric Physics, Research Institute of Physics, St. Petersburg State University, Ulyanovskaya Str. 1, 198904 St. Petersburg, Russia.

J.-C. Lambert, G. Pinardi, and M. van Roozendael, Chemistry and Physics of Atmospheres, Federal Space Pole, Belgian Institute for Space Aeronomy, 3 Avenue Circulaire, B-1180 Brussels, Belgium.

G. Mount and E. Spinei, Laboratory for Atmospheric Research, Department of Civil and Environmental Engineering, Washington State University, Pullman, WA 99164-2910, USA.

A. Richter, A. Schönhardt, and F. Wittrock, Institute for Environmental Physics, University of Bremen, D-28334 Bremen, Germany.

D. P. J. Swart, Netherlands National Institute for Public Health and the Environment (RIVM), Postbus 1, NL-3720 BA Bilthoven, Netherlands.

T. Wagner, Max-Planck-Institute for Chemistry, D-55128 Mainz, Germany.